Solar Water Splitting Cells

Michael G. Walter, Emily L. Warren, James R. McKone, Shannon W. Boettcher,[†] Qixi Mi, Elizabeth A. Santori,
and Nathan S. Lewis*

Division of Chemistry and Chemical Engineering, 210 Noyes Laboratory, 127-72 California Institute of Technology, Pasadena, California 91125

Contents

* Corresponding author. E-mail: nslewis@caltech.edu.
† Current address: Department of Chemistry, University of Oregon, Eugene OR 97403.

1. Introduction

Energy harvested directly from sunlight offers a desirable approach toward fulfilling, with minimal environmental impact, the need for clean energy. Solar energy is a decentralized and inexhaustible natural resource, with the magnitude of the available solar power striking the earth's surface at any one instant equal to 130 million 500 MW power plants.[1] However, several important goals need to be met to fully utilize solar energy for the global energy demand. First, the means for solar energy conversion, storage, and distribution should be environmentally benign, i.e. protecting ecosystems instead of steadily weakening them. The next important goal is to provide a stable, constant energy flux. Due to the daily and seasonal variability in renewable energy sources such as sunlight, energy harvested from the sun needs to be efficiently converted into chemical fuel that can be stored, transported, and used upon demand. The biggest challenge is whether or not these goals can be met in a cost-effective way on the terawatt scale.[2]

Collecting and storing solar energy in chemical bonds, as nature accomplishes through photosynthesis, is a highly desirable approach to solving the energy challenge. The "Holy Grail" of solar energy conversion and storage is the photoelectrolysis of water using semiconductors as both the light absorber and energy converter, to store solar energy in the simplest chemical bond, H_2.[3] Efficiently splitting water into usable hydrogen could become a new industrial photosynthesis that would provide clean fuel whose only waste product upon utilization is water. To accomplish this new photosynthesis, an economically viable water splitting cell, composed of stable semiconductors designed to split water directly at the semiconductor surface, needs to be developed.[4] Photoelectrolysis can also be accomplished using photovoltaic (PV) modules connected directly to electrolyzers and/or catalytic electrodes. Water splitting cells with direct semiconductor/liquid contacts are attractive because they avoid significant fabrication and systems costs involved with the use of separate electrolyzers wired to p−n junction solar cells.[5] Another attractive advantage of photoelectrochemical water splitting directly at the semiconductor surface is the ease with which an electric field can be created at a semiconductor/liquid junction.[6]

Michael G. Walter earned a B.S. degree in chemistry from the University of Dayton in 2001 and as an undergraduate worked on conductive polymer syntheses at the Air Force Research Laboratory at Wright Patterson Air Force Base. He completed an M.S. degree in 2004 and Ph.D. degree in 2008 at Portland State University and joined the Lewis group at Caltech in 2008. He is currently an NSF-ACCF postdoctoral fellow (2009) and has been studying the electrical characteristics of inorganic semiconductors in contact with conductive polymers. His research interests include molecular semiconductors for solar energy conversion, porphyrin macrocycles for optoelectronic applications, and catalyst materials for photoelectrolysis.

Emily L. Warren received a B.S. in chemical engineering at Cornell University in 2005. She received an M.Phil in Engineering for Sustainable Development from Cambridge University in 2006. She is currently a graduate student in Chemical Engineering at the California Institute of Technology. Her research interests include semiconductor photoelectrochemistry, solar energy conversion, and semiconductor nanowires. She is currently a graduate student in Chemical Engineering at the California Institute of Technology, working under Nathan S. Lewis.


James R. McKone is in his third year of graduate studies in the Division of Chemistry and Chemical Engineering at the California Institute of Technology, working under Nathan S. Lewis and Harry B. Gray. In 2008 he graduated from Saint Olaf College with a Bachelor of Arts degree, double-majoring in music and chemistry. His current research focuses on semiconductor-coupled heterogeneous catalysis of the hydrogen evolution reaction using mixtures of earth-abundant transition metals.

Shannon W. Boettcher earned his B.A. degree in chemistry from the University of Oregon, Eugene (2003), and, working with Galen Stucky, his Ph.D. in Inorganic Chemistry from the University of California, Santa Barbara (2008). Following postdoctoral work with Nate Lewis and Harry Atwater at the California Institute of Technology (2008−2010), he returned to the University of Oregon to join the faculty as an Assistant Professor. His research interests span synthesis and physical measurement with the goal of designing and understanding solid-state inorganic material architectures for use in solar-energy conversion and storage.

In the nearly 40 years since Honda and Fujishima's electrochemical photolysis report using TiO_2,[7] the approach to solving the water splitting problem has been focused on evaluating new materials for both anodic/cathodic processes and integrating configurations that utilize photovoltaic cell junctions, to increase the obtainable voltage for a single or dual band gap device. The ultimate goal of these efforts is an efficient photoelectrolysis cell design that can simultaneously drive, in an unassisted fashion, both the hydrogen evolution and water oxidation reactions. Water splitting cells require semiconductor materials that are able to support rapid charge transfer at a semiconductor/aqueous interface, that exhibit long-term stability, and that can efficiently harvest a large portion of the solar spectrum. To achieve these functions, multijunction configurations that use p- and n-type semiconductors with differing band gaps, and surface bound electrocatalysts, have been the predominant approach for the development of efficient photoelectrolysis cells.[8]

This review will focus on the efforts to develop an efficient semiconductor-based photoelectrochemical water splitting device in which the only inputs are sunlight and water.[9] The fundamental principles of photoinduced electron-transfer mechanisms at a semiconductor/liquid junction, and optimization of such processes, will be summarized. A wide range of both p- and n-type semiconductor photoelectrode materials that have been studied for photoelectrochemical water splitting cells will then be described. In addition, heterogeneous electrocatalysts used to facilitate the oxidation and reduction reactions in electrochemical and in photoelectrochemical water splitting systems will be reviewed. Finally, efforts to combine photoanode, photocathode, and photovoltaic-assisted coupled configurations in both single and dual band gap photoelectrolysis cells will be examined in terms of their solar-to-hydrogen (STH) efficiency, stability, and expected viability. Strategies to optimize solar-to-chemical energy-conversion efficiencies by optimization of
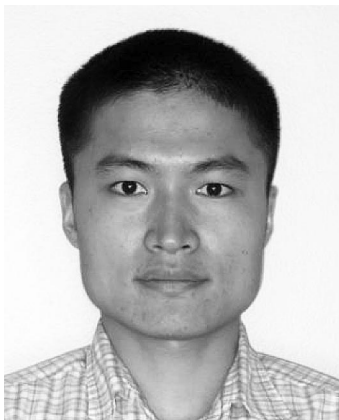
Qixi Mi obtained his B.S. at Peking University in 2003 and Ph.D. at Northwestern University in 2009. He is currently a postdoctoral fellow of the NSF Center for Chemical Innovation (CCI Solar) at Caltech, working on the development of novel photoanode materials for water oxidation using visible light, under the supervision of Profs. Nathan S. Lewis and Harry B. Gray.

Elizabeth Santori received a B.S. in chemistry from the University of Chicago in 2007. She is currently a graduate student in chemistry at the California Institute of Technology in Prof. Lewis's lab. Research interests include structured semiconductors for photocatalysis and catalysis for water oxidation.

light harvesting structured semiconductors, photoinduced electron transfer and transport, and surface catalysis will also be described.

2. Photoelectrolysis

The free energy change for the conversion of one molecule of H_2O to H_2 and $1/2$ O_2 under standard conditions is $\Delta G = 237.2$ kJ/mol, which, according to the Nernst equation, corresponds to $\Delta E° = 1.23$ V per electron transferred. To use a semiconductor and drive this reaction with light, the semiconductor must absorb radiant light with photon energies of >1.23 eV (equal to wavelengths of ~1000 nm and shorter) and convert the energy into H_2 and O_2. This process must generate two electron−hole pairs per molecule of H_2 (2×1.23 eV = 2.46 eV) or four electron−hole pairs per molecule of O_2 (4×1.23 eV = 4.92 eV). In the ideal case, a single semiconductor material having a band gap energy (E_g) large enough to split water, and having a conduction band-edge energy (E_{cb}) and valence band-edge energy (E_{vb}) that straddles the electrochemical potentials $E°$ (H^+/H_2) and $E°$ (O_2/H_2O), can drive the hydrogen evolution reaction (HER) and oxygen evolution reaction (OER) using electrons/holes generated under illumination (Figure 1).
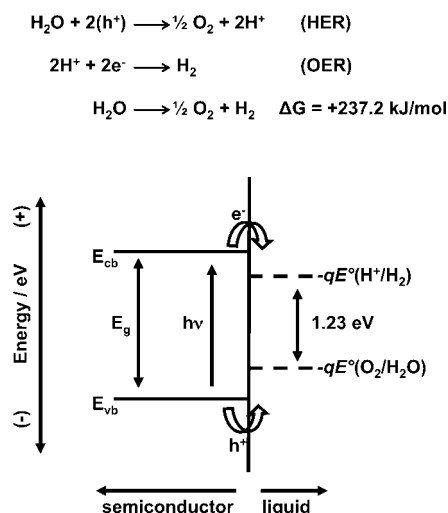
Dr. Nathan Lewis, George L. Argyros Professor of Chemistry, has been on the faculty at the California Institute of Technology since 1988 and has served as Professor since 1991. He has also served as the Principal Investigator of the Beckman Institute Molecular Materials Resource Center at Caltech since 1992, is the Principal Investigator of the Joint Center for Artificial Photosynthesis, the DOE's $122 MM Energy Innovation Hub in Fuels from Sunlight. From 1981 to 1986, he was on the faculty at Stanford, as an assistant professor from 1981 to 1985 and as a tenured Associate Professor from 1986 to 1988. Dr. Lewis received his Ph.D. in Chemistry from the Massachusetts Institute of Technology. He has been an Alfred P. Sloan Fellow, a Camille and Henry Dreyfus Teacher-Scholar, and a Presidential Young Investigator. He received the Fresenius Award in 1990, the ACS Award in Pure Chemistry in 1991, the Orton Memorial Lecture award in 2003, the Princeton Environmental Award in 2003 and the Michael Faraday Medal of the Royal Society of Electrochemistry in 2008. He is currently the Editor-in-Chief of Energy & Environmental Science. He has published over 300 papers and has supervised approximately 60 graduate students and postdoctoral associates. His research interests include artificial photosynthesis and electronic noses. Technical details of these research topics focus on light-induced electron transfer reactions, both at surfaces and in transition metal complexes, surface chemistry and photochemistry of semiconductor/liquid interfaces, novel uses of conducting organic polymers and polymer/conductor composites, and development of sensor arrays that use pattern recognition algorithms to identify odorants, mimicking the mammalian olfaction process.

To carry out one or both reactions without recombination, photoinduced free charge carriers (electrons and holes) in the semiconductor must travel to a liquid junction, and must react only with solution species directly at the semiconductor surface. The electron-transfer processes at semiconductor/liquid junctions produce losses due to the concentration and kinetic overpotentials needed to drive the HER and the OER. The energy required for photoelectrolysis at a semiconductor photoelectrode is therefore frequently reported as 1.6−2.4 eV per electron−hole pair generated, to account for these losses.[5,10] The surface properties of these liquid/semiconductor interfaces, and how these properties affect the energetics of photoelectrolysis, will be explored further in section 3. The practical need for 1.6−2.4 eV to effectively drive water splitting motivates the use of multiple semiconductors with different energy gaps, as described in the next section.

2.1. Theoretical Efficiencies for Water Splitting Cells

Bolton classified solar water splitting themes, and estimated their overall efficiencies, based on the number of photosystems (semiconductor materials) and the minimum number of absorbed photons per H_2 molecule. For example, a single semiconductor material with a band gap of 1.6 eV (threshold wavelength = 775 nm) has an ideal maximum conversion efficiency at 1 Sun of 30%. This system is given the classification of **S2** to indicate a single band gap device

$$H_2O + 2(h^+) \longrightarrow \tfrac{1}{2} O_2 + 2H^+ \qquad (HER)$$

$$2H^+ + 2e^- \longrightarrow H_2 \qquad (OER)$$

$$H_2O \longrightarrow \tfrac{1}{2} O_2 + H_2 \qquad \Delta G = +237.2 \text{ kJ/mol}$$

Figure 1. Oxygen evolution reaction (OER) and hydrogen evolution reaction (HER) for overall water splitting (under acidic conditions); ideal semiconductor material for splitting water at its surface under illumination with absolute energy scale represented [left vertical axis (−) and (+)] for E_{cb} and E_{vb} and the electrochemical potentials given by $-qE°$, where $E°$ is the reduction potential for both (H⁺/H₂) and (O₂/H₂O) redox couples.

requiring two photons to produce one molecule of H_2.[10] The theoretical efficiency is based upon the conversion of incident solar energy to chemical energy, eq 1:

$$\eta = \frac{J_g \mu_{ex} \phi_{conv}}{S} \qquad (1)$$

where J_g is the absorbed photon flux, μ_{ex} is the excess chemical potential generated by light absorption, ϕ_{conv} is the quantum yield for absorbed photons, and S is the total incident solar irradiance (mW cm^{-2}).

A dual band gap configuration is given the classification of (**D2**) or (**D4**), indicating a system that requires two or four photons to produce one molecule of H_2, respectively. A dual band gap (**D4**) solar water splitting system, realized by stacking two materials in tandem, has an *ideal* theoretical efficiency of 41% using the same theoretical basis used for **S2**.[10] The *chemical* conversion efficiency for a dual band gap (**D4**) system is 27% when including losses due to the fraction of unused energy per absorbed photon (about 0.8 eV). In this scenario, the two semiconductor materials have complementary absorption characteristics, such that the top layer has a band gap of 1.7 eV (730 nm) and the bottom layer absorbs longer wavelengths, 1.1 eV (1120 nm). If the two materials were illuminated side-by-side, an increase in the illuminated area lowers the overall photocurrent density resulting in an overall efficiency that reflects the area-weighted average of two **S2** photosystems.[10]

The theoretical limits presented for **S2** and **D4** systems do not account for losses in current efficiencies that are caused by nonradiative recombination of photogenerated electron−hole pairs in the semiconductor bulk, or for losses due to the overpotentials required to drive the HER and OER at the electrode surfaces. The overpotentials required to drive water oxidation and reduction are especially important for placement of the valence-band and conduction-band edge positions of a semiconductor relative to the potentials for the oxygen and hydrogen evolution reactions, respectively.[11] A valence band whose potential is not sufficiently positive, for water oxidation, or whose conduction band is not
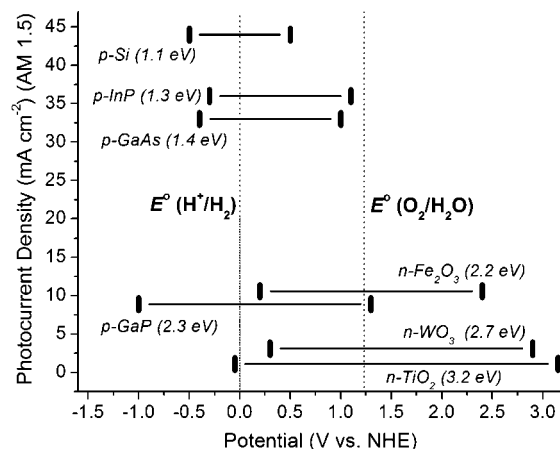
Figure 2. Conduction band (left bar) and valence band (right bar) positions vs NHE of common semiconductors used in photoelectrolysis cells. The band gap value is in parentheses, and the ordinate indicates the maximum theoretical photocurrent under Air Mass 1.5 illumination. The dotted lines indicate the thermodynamic potentials for water reduction and oxidation, respectively.

sufficiently negative, for proton reduction, can lead to slow or negligible water splitting.[11] Overpotentials of 400 mV at 10 mA cm^{-2} for water oxidation and 50 mV at 10 mA cm^{-2} for H_2 evolution at a semiconductor/liquid junction are useful starting points for estimating how efficiently a photoelectrode can drive the OER or HER.[11]

Figure 2 presents the band-edge positions vs the normal hydrogen electrode (NHE) for several common p- and n-type semiconductor materials. The semiconductor band-edge positions are plotted versus their integrated maximum photocurrent under Air Mass 1.5 illumination, in the conventional Shockley−Quiesser limit for solar energy conversion.[12,13] Some of the large band gap n-type semiconductors in Figure 2 straddle the potentials of the O₂/H₂O redox couple, but these materials are not capable of producing high photocurrent densities under AM 1.5 illumination. In contrast, the smaller band gap (higher photocurrent) p-type materials shown in Figure 2 have more negative conduction/valence bands that are well suited to effect reactions at the H⁺/H₂ potential. A dual band gap (**D4**) cell configuration would connect, in series, an n-type material having a sufficiently positive valence band to drive water oxidation with a reasonable photocurrent, with a smaller band gap, p-type semiconductor that would drive the hydrogen evolution reaction. The use of two semiconductor materials (**D4**) remains an attractive option for capturing a large portion of the solar spectrum, with the two band gaps tuned to absorb complementary portions of the solar spectrum.[14] Solar-to-hydrogen efficiencies of 15% have been calculated for a model dual band gap tandem p/n photoelectrolysis cell (p/n-PEC), including losses associated with mass-transport and kinetic overpotentials.[11] Energy conversion devices that utilize multiple semiconductors with different band gaps can achieve higher efficiencies, as will be discussed in section 6.

In addition to exhibiting an optimal band gap for solar absorption, semiconductor photoelectrodes must exhibit excellent oxidative/reductive stability in contact with aqueous electrolyte solutions. For thermodynamic stability, a semiconductor's reductive and oxidative decomposition potentials must be more negative than the semiconductor's conduction band-edge for water reduction or more positive than the semiconductor valence band-edge potential for water oxida-

tion, respectively. Very few semiconductor materials exhibit the necessary requirements for electrode stability in aqueous electrolyte solutions simultaneously for both water oxidation and reduction.[15]

2.2. Calculation of Solar-to-Chemical Conversion Efficiencies

Efficiencies for water splitting photoelectrode devices that require an external bias in order to drive water electrolysis can be calculated using eq 2 (assuming no corrosion reaction at the photoelectrodes and a Faradaic efficiency of unity for both reactions). In order to obtain a true systems efficiency, these measurements should be done in a two-electrode configuration as opposed to a three-electrode electrochemical cell. The efficiency (η) can be calculated from $J-V$ data using eq 2:

$$\eta = \frac{J_{mp}(1.23V - V_{app})}{P_{in}} \quad (2)$$

with V_{app} as the applied voltage measured between the oxygen-evolving photoanode and the hydrogen-evolving photocathode, J_{mp} as the externally measured current density, and P_{in} as the power density of the illumination. In this scenario, products must be separated to ensure that the reverse reactions are suppressed, e.g. oxidation of H_2 at the photoanode leading to erroneous cell measurements. For an integrated device (back-to-back photoelectrodes) with no external wiring, the efficiency must be calculated by physically collecting the generated products, e.g. hydrogen and oxygen, and relating the free energy contained in the chemical products to the energy of the incoming light.[14b,16] Using eq 2, a true solar-to-hydrogen (STH) production efficiency, where the only inputs are sunlight and water, can be calculated by measuring the photocurrent (J_{mp}) at $V_{app} = 0$ V (under short-circuit conditions).

The solar conversion efficiency of individual candidate photoelectrode materials that might be used in a multiple band gap photoelectrolysis cell to drive either the HER or OER can be calculated from current–voltage data obtained using a potentiostat in an illuminated three-electrode cell. It is useful to calculate efficiencies of a photoanode or photocathode separately from the other half of the water splitting reaction, to allow for optimization of the materials independently. It is important to recognize that characterizing individual photoelectrodes by the power produced represents only a portion of the Gibbs free energy needed to split water.[8c,17] Therefore, the open-circuit voltage (V_{oc}) and short-circuit current density (J_{sc}) are referenced to the thermodynamic potential of the water splitting reactions (H^+/H_2, O_2/H_2O) at a specific pH. The efficiency (η) of a photoelectrode can be calculated from its current–voltage data using eq 3, where J_{mp} is the current density at the maximum power point (P_{PA}),

$$\eta = \frac{J_{mp}V_{mp}}{P_{in}} \qquad P_{PA} = J_{mp}V_{mp} \qquad ff = \frac{I_{mp}V_{mp}}{I_{sc}V_{oc}} \quad (3)$$

V_{mp} is the voltage at the maximum power point, and P_{in} (in W cm^{-2}) is the power of the incoming illumination. The fill factor (ff) is calculated using the open-circuit potential V_{oc} and the value of J_{sc} with respect to the desired half-reaction.
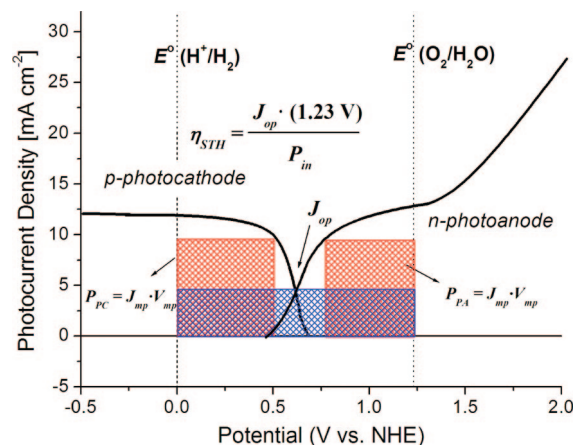
Figure 3. Overlaid current density-potential behavior for a p-type photocathode and an n-type photoanode, with overall efficiency projected by the power generated $P_{STH} = J_{op}$ (1.23 V) by the cell for splitting water.

The ff is defined as the maximum power output divided by the product of the open circuit voltage and the short-circuit current density. Further details examining the physical phenomena associated with the ff characteristics for a photoelectrochemical cell have been rigorously studied and are most closely related to surface recombination of electrons/holes, bulk recombination in the semiconductor, and uncompensated solution resistances.[18] These topics will be covered in greater detail in section 3.

Calculations based on eq 3 are identical to an efficiency calculation for a photovoltaic cell. However, because the potentiostat is operated in three-electrode mode, polarization losses associated with driving the reaction at the counter electrode are not taken into account in the calculation. Hence, calculated efficiencies represent only photoanode or photocathode efficiencies and not overall efficiencies for water splitting (STH).

By independently characterizing photoanodes and photocathodes, the expected performance of an integrated system with no external electronics can be directly calculated. Overall water splitting efficiencies (STH) for photoelectrolysis cells can be estimated by overlapping the individually tested $J-V$ data for each photocathode/anode (Figure 3).[11,19] The intersection of the two curves indicates the maximum operating current density (J_{op}) for the complete cell. The highest efficiency for a p/n-photoelectrochemical cell (PEC) will be obtained when the two curves intersect closest to their individual maximum power points (P_{PC} or $P_{PA} = J_{mp} \cdot V_{mp}$, maximum power for photoanode P_{PA} or photocathode P_{PC}). A theoretical p/n-PEC photoanode/photocathode device is depicted in Figure 3, illustrating the power generated for each component of the cell (red shaded area) and the power generated at the maximum operating current density (blue shaded area).

Increasing the fill factor for one or both of the photoelectrodes has a dramatic effect on the solar-to-hydrogen efficiencies, due to the steep increase in operating photocurrent densities that are produced by small changes in the fill factor.[11,20] For a p/n dual band gap photoelectrolysis cell, increases in the fill factor (from 0.5 to 0.7) for both the photocathode and the photoanode increased the calculated overall solar-to-hydrogen efficiency from 10% to 15%.[11] If the two curves do not cross, i.e. $J_{op} \leq 0$, the serial combination of electrodes will not drive the photoelectrolysis of water.

Because the voltage generated under illumination is a key parameter for describing the efficiencies of semiconductor photoanodes and photocathodes, proper measurement of the photovoltage is important. Several practical steps should be taken when measuring the V_{oc} of an individual photoelectrode to be used in a water splitting cell. For a photocathode system, e.g. p-InP decorated with platinum catalyst particles,[8c] measurement of V_{oc} is achieved by submerging the photoelectrode in electrolyte bubbled with pure hydrogen, and measuring the voltage under illumination versus a clean Pt electrode that serves as a reversible hydrogen electrode (RHE) reference in a three-electrode electrochemical cell. To accurately measure V_{oc} for an H_2-evolving photocathode, it is important to have both the oxidized and reduced species present at the electrode; therefore, H_2 must be present in the solution. Because platinum is a good catalyst for both H^+ reduction and H_2 oxidation, the Pt reference rapidly equilibrates to the thermodynamic potential for hydrogen evolution in the specific electrolyte of interest. A standard calomel or silver chloride reference electrode can be used as well, provided that the reversible hydrogen evolution potential is first measured in the same solution using a clean Pt electrode, and the final data are referenced to the explicitly measured RHE potential. Bubbling hydrogen at 1 atm during $J-E$ data collection maintains constant H^+/H_2 concentrations in solution, ensuring a well-defined Nernstian potential with which the semiconductor can equilibrate. This situation also approximates that of an actual working device, because under operating conditions, H_2 is generated continuously at the electrode surface, causing the solution to locally saturate with the evolved gas. Measurement of V_{oc} without bubbling H_2, even versus a standard reference such as the saturated calomel, will produce an incorrect photovoltage, due to a poorly defined solution potential (i.e., with no hydrogen present, the potential of the H^+/H_2 redox couple is undefined, per the Nernst equation.

A similar method should be used for the measurement of the V_{oc} for n-type photoanodes for oxygen evolution. In this case, the electrode should be submerged in the electrolyte, O_2 should be bubbled through the solution, and a standard reference electrode should be used (due to the relative difficulty in using the oxygen couple as a reference). The voltage is measured under these standard conditions versus the reference, and then converted to a scale based upon the actual O_2/H_2O potential, which can be calculated from the pH of the solution. Current–voltage data should be recorded under 1 atm of bubbling O_2 to yield correct V_{oc} values.

In addition, for measuring both photocathodes and photoanodes, ultrahigh purity electrolytes should be used, and can be produced from standard reagent grade salts and buffers, via overnight pre-electrolysis using two large, inert electrodes such as platinum or carbon.[21] Overnight pre-electrolysis can remove organic impurities and trace metals through oxidation/reduction, respectively. Note, however, that if Pt electrodes are used for pre-electrolysis, small amounts of dissolved Pt can enter the electrolyte, which can become problematic when studying non-noble catalysts.

## 2.3. Photoelectrolysis Cell Configurations

A basic photoelectrochemical water splitting device can be constructed from a single p-type or n-type semiconductor, i.e. as a single band gap device (**S2**) or from two semiconductors connected in series, i.e. a dual band gap device - p/n-PEC (**D4**). As mentioned in section 2.2, a single band

gap device requires, at a minimum, a semiconductor with a 1.6 to 1.7 eV band gap in order to generate the V_{oc} required to split water, though once other voltage-loss mechanisms (i.e., catalysis) are accounted for, a band gap above 2 eV is generally necessary.[11] To obtain efficient water splitting devices using currently available semiconductor materials, a **D4** photoelectrolysis cell configuration is advantageous, due to the ability to explore various combinations of smaller band gap semiconductor materials that have complementary absorption and stability characteristics.[10,11] A dual band gap photoanode/cathode configuration also allows for a higher obtainable photovoltage, while partitioning the water splitting half-reactions between two semiconductor/liquid interfaces. Another approach to a dual band gap cell uses a single photocathode/anode in series with a PV cell layer that provides the additional bias needed to drive the water splitting reactions. Regardless of the configuration, semiconductor/liquid junctions in these devices present unique challenges to sustain the necessary photovoltages for driving the reactions at the photocathode and the photoanode. Multiple semiconductor layers within the cell also incur losses due to reflected or scattered photons at junctions, thereby lowering the overall system performance.

Figure 4 depicts the basic configurations with a single (Figure 4a) or dual band gap (Figure 4b–d) photoelectrochemical cell device structure utilizing a back-to-back "wireless" design that was first pursued by Nozik in a "photochemical diode" using a p/n-PEC device configuration.[14b] These configurations can also be evaluated in separate electrochemical cells, allowing for the testing and characterization of individual photoelectrodes. A back-to-back wireless configuration has the potential to be incorporated into a low-cost, manufacturable device structure. The single band gap cell depicted in Figure 4a can be constructed using a p-type photocathode for hydrogen evolution, electrically connected to an oxygen-evolving metal electrode. Many known p-type semiconductors that have high absorption in the visible region of the solar spectrum do not have valence band-edge potentials that are sufficiently positive to oxidize water. Therefore, photoelectrolysis cells using one type of photoelectrode (photocathode or photoanode) can include a PV cell, connected in series to supply the extra needed bias voltage. Figure 4c depicts an n-type photoanode electrolysis cell with a buried p–n junction PV layer connected directly to the photoelectrode, along with the relative band energetics of these components with respect to the hydrogen and oxygen evolution reactions.

In the cell configurations in (Figure 4a–c), minority charge carriers generated under illumination (holes in n-type semiconductor photoanodes and electrons in p-type semiconductor photocathodes) are driven to the semiconductor/aqueous solution interface as a result of the electric field formed at the semiconductor/liquid contact. Majority carriers recombine at ohmic contacts that connect the photoelectrodes, or are transferred to a metal cathode/anode and carry out the complementary photoelectrolysis step. In the n-type photoanode/PV cell (Figure 4c), majority carriers generated in the PV cell reduce protons in solution on a metal cathode and minority holes generated in the n-type photoelectrode oxidize water at its surface.

A dual band gap p/n-PEC (Figure 4b) utilizes both electron and hole minority charge carriers for water splitting reactions at their respective semiconductor/liquid interfaces. This is in contrast to Figure 4d, which depicts two p–n PV cells
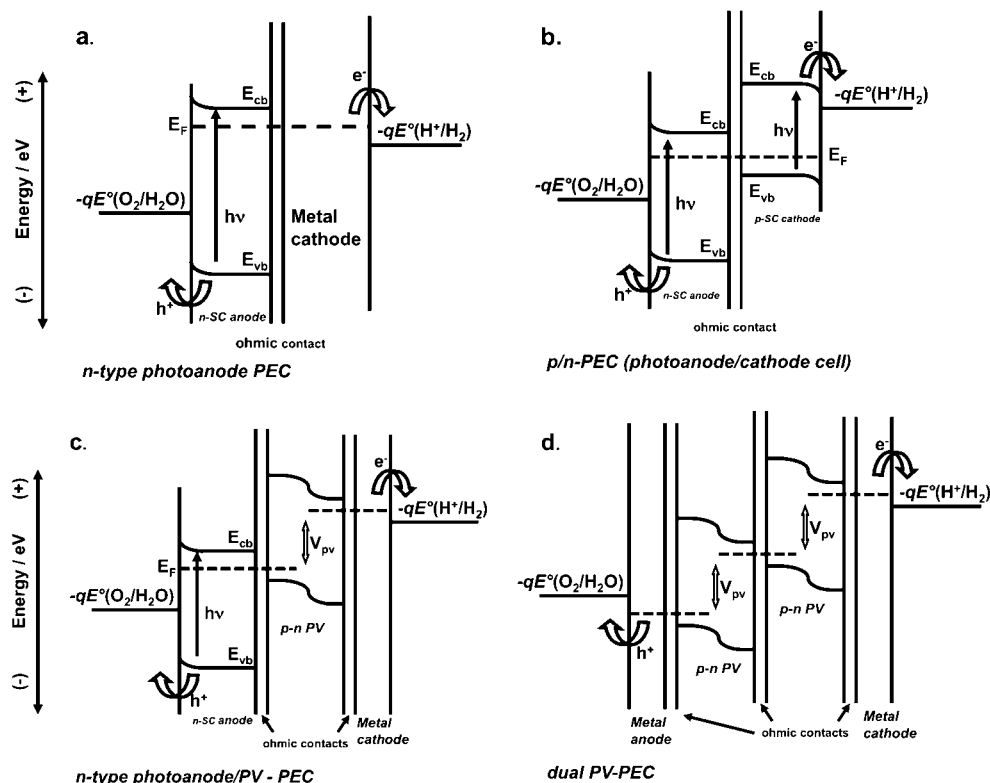
Figure 4. Energy diagrams for (a) a single band gap photoanode (n-SC = n-type semiconductor) PEC with metal cathode back contact; (b) a dual band gap p/n-PEC configuration with n-type and p-type photoelectrodes electrically connected in series; (c) n-type photoelectrode in series with an integrated p−n PV cell to provide additional bias and connected to a metal cathode for hydrogen evolution; (d) two p−n PV cells connected in series and integrated into a metal cathode and anode for water oxidation and reduction.

connected in series and coated with a metal cathode and anode. In this configuration, the majority carriers are injected from the PV cells into the metal cathode and anode to carry out water reduction and oxidation, respectively.[14b] PV cells integrated directly into water splitting cathodes and anodes are termed "buried" photoelectrochemical junctions, because no direct liquid/semiconductor junction is formed. Devices containing buried junctions can be classified as photovoltaic photoelectrolysis cells (PV-PEC), and are essentially identical to configuring multiple PV cells wired directly to an electrolyzer.[22] The semiconductor surfaces in these configurations can be completely protected from the aqueous solution using evaporated metal electrodes or thin oxide layers. The junctions that provide the driving force for splitting water are therefore buried, and are not directly related to the difference between the redox potentials of the H$^+$/H$_2$ or the O$_2$/H$_2$O redox couples or the conduction/valence band-edge positions, respectively, of the semiconductor photoelectrode.[23] This type of system encompasses many reported PEC cell configurations that are composed of multi band gap, buried p−n junction photoelectrodes, and does not show semiconductor/liquid junction device properties that have been described in the next section.[24]

3. Semiconductor Photoelectrochemistry

To design an efficient solar water splitting cell, it is critical to understand the fundamental device physics of semiconductors, the thermodynamic and kinetic parameters of semiconductor−liquid contacts, and the function of surface electrocatalysts. Several introductory books and reviews that address semiconductor device physics are suitable for chemists and materials scientists.[25] Several reviews also address the photovoltaic performance of semiconductors in contact

with fast, reversible redox couples (i.e., so-called regenerative cells).[25c,26] This section aims to present a concise view of photoelectrochemical semiconductor/liquid contacts, utilizing the well-developed concepts presented in these earlier books and reviews. The physics of the semiconductor/liquid contact under equilibrium conditions will be discussed in section 3.1, while efforts to optimize the interfacial kinetics of photoelectrolysis, such the functionalization of the semiconductor surface with dipoles, are presented in section 3.2. Finally an analysis of the photogenerated charge carrier pathways and their effect on the obtainable voltage of an illuminated semiconductor is presented in section 3.3.

3.1. Physics of Semiconductor/Liquid Contacts

When a semiconductor is brought into contact with a liquid that contains a redox couple (consisting of the acceptor, A, and the donor, A$^-$) having electrochemical potential $-qE°$(A/A$^-$) where $E°$ is the Nernst potential of the redox pair (A/A$^-$), electrons will flow between the semiconductor and the solution until equilibrium is established (Figure 5). Charge transfer results in an interfacial electric field whose electrostatic potential balances the initial difference in electrochemical potentials between the solution and semiconductor. After equilibration, the electrochemical potential (Fermi level) is the same everywhere. For a photoelectrochemical water splitting device, the redox couples of interest are the H$^+$/H$_2$ couple for a p-type semiconductor photocathode, and the O$_2$/H$_2$O couple for an n-type semiconductor photoanode.

For a typical n-type semiconductor photoanode in equilibrium with a redox species in solution (e.g., O$_2$/H$_2$O), the electrode will have an excess positive charge, arising from the ionized dopant atoms in the semiconductor, and the solution will have an excess negative charge. The positive

A. Before equilibrium   **B. After equilibrium**   **C. Illuminated**
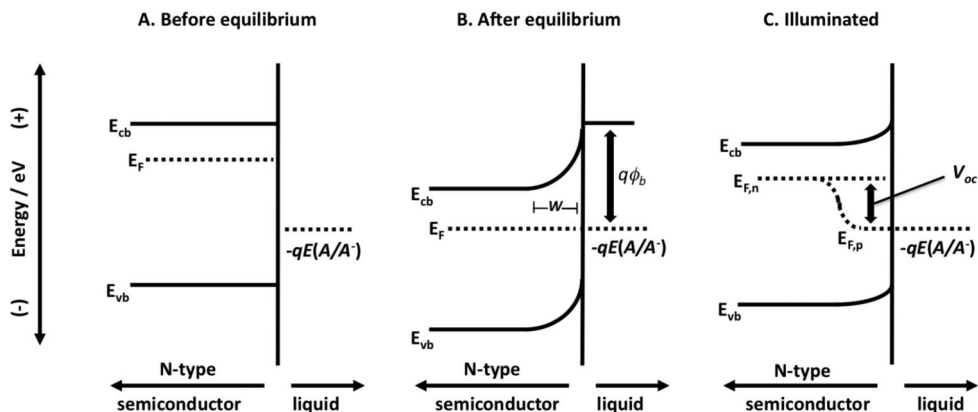
Figure 5. The band energetics of a semiconductor/liquid contact are shown in three cases: (A) before equilibration between the two phases; (B) after equilibration, but in the dark; and (C) in quasi-static equilibrium under steady state illumination (discussed in section 3.3). In panel B, $q\phi_b$ is known as the barrier height, and its magnitude determines the theoretical maximum energy that can be extracted from a separated electron−hole pair at the semiconductor/liquid junction. In panel C, where steady-state illumination yields nonequilibrium electron and hole populations, $E_{F,n}$ is the electron quasi-Fermi level and $E_{F,p}$ is the hole quasi-Fermi level. The voltage generated by the junction under illumination is given by the difference between $E_{F,n}$ and $-qE(A/A^-)$.

charge is spread out over the depletion width, W, in the semiconductor, whereas the negative charge is spread over a much narrower region (the Helmholtz layer) in solution, close to the electrode. An N-type semiconductor is traditionally used as a photoanode because the electric field that is developed in equilibrium with a redox couple results in band bending, due to the drop in the electric field strength in the solid, that directs photogenerated free minority charge carriers (holes, for n-type semiconductors) to move into the solution.[26a] P-type semiconducting electrodes behave in an analogous manner, except that the ionized dopants are negatively charged and the solution is positively charged. Therefore, p-type semiconductors favor electron flow into the positively charged acceptor species at the interface.

The electric field strength and, hence, the potential energy barrier in the semiconductor, depend on the initial energy difference between the Fermi level of the semiconductor and the value of $-qE(A/A^-)$. Because the initial difference in electrochemical potentials is on the order of 1 eV, and the depletion width in the semiconductor is typically on the order of hundreds of nanometers, the electric field in the semi-conductor can be as large as 10^5 V cm^{-1}.[26a] Charge carriers (electron−hole pairs) generated by the absorption of light are generally very effectively separated by this electric field, because of the relatively large mobilities of charge carriers (10−1000 cm^2 V^{-1} s^{-1}) in crystalline inorganic semiconductors.

3.2. Optimization of Interfacial Energetics for Photoelectrolysis Systems

The theoretical limit on the efficiency of a photoelectrode is determined by the energy that can be extracted from the photogenerated electron−hole pairs. In principle, the maximum internal energy that can be extracted from these pairs for an n-type photoanode is given by the difference between E_{cb} and $-qE(A/A^-)$, that is, the barrier height ($q\phi_b$ in Figure 5b). To optimize performance of a semiconductor/liquid junction, this difference should be as large as possible.

In a regenerative photoelectrochemical cell, the efficiency of energy extraction can be optimized for a given semiconductor by varying the electrochemical potential of the redox system. For example, a series of studies has shown that, for well-defined semiconductor surfaces, such as Si and InP in nonaqueous solvents, systematic tuning of the redox potential

provides a method for chemically controlling, and optimizing, the interfacial barrier height.[27]

In a photoelectrolysis cell, however, the redox couple is fixed by the desired chemistry, i.e. water oxidation and reduction. Therefore, the interface energetics cannot be tuned by simply selecting the appropriate redox couple. However, the same fundamental limits to energy extraction apply in a photoelectrolysis cell as in a regenerative photovoltaic cell. In principle, in water splitting devices several routes could allow for tuning the relative semiconductor−solution energetics. For example, the redox potentials for water oxidation (and reduction) are pH dependent, eq 4.

$$2H_2O + 4(h^+) \rightarrow O_2 + 4H^+$$
$$E°(O_2/H_2O) = 1.23 \text{ V} - 0.059 \text{ V} \times \text{pH (vs NHE)}$$

$$(4)$$
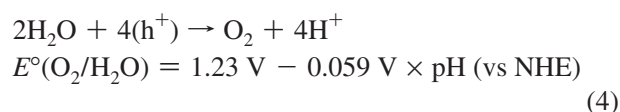
This behavior suggests that the relative energetics of the semiconductor−solution interface can be tuned by simply adjusting the pH of the solution. Unfortunately, this tactic has been largely unsuccessful. The surfaces of semiconductor electrodes in contact with water are typically covered with hydroxyl groups. As the pH changes, these surface groups protonate/deprotonate, resulting in a pH-dependent surface dipole.[28] This surface dipole generates a potential drop that shifts the bands in unison with the shifting water reduction and oxidation potentials (i.e., ~60 mV per pH unit). Because both the oxide band edge and the redox couple are pH sensitive, the relative interfacial energetics remain pH independent. One a strategy to circumvent this problem is to functionalize the semiconductor surface with a pH insensitive organic group, to thereby produce a surface dipole that is no longer pH dependent (such as methylated silicon).[29] It has yet to be shown, however, that such a strategy is suitable for photoelectrosynthetic cells that must also incorporate electrocatalysts.

Another promising approach is to operate at a set pH, and to directly tune the band edge positions relative to the water oxidation or reduction potentials via the incorporation of fixed dipoles or charges on the semiconductor surface (Figure 6).[26d] These dipoles/charges must be held very close to the surface of the semiconductor, to avoid screening by the electrolyte solution. Turner and co-workers demonstrated that

A. Bare Interface

B. "Negative" Dipole

C. "Positive" Dipole
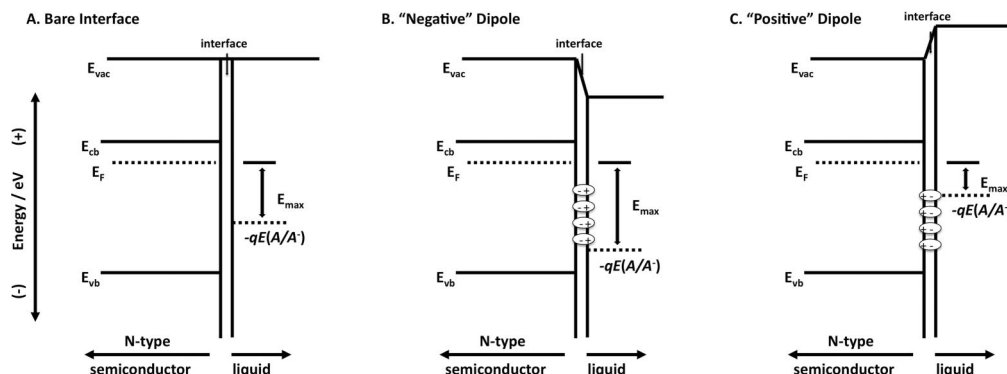
Figure 6. The presence of an interfacial dipole layer in panels B and C can significantly affect the electrostatic barrier ($q\phi_b$) and hence the photoelectrode performance. For simplicity, the band diagrams are shown at the flat-band condition in the absence of band bending. E_{vac} is the energy of an isolated electron in vacuum and E_{max} represents the theoretical maximum energy that can be extracted from an electron−hole pair.

the chemical functionalization of GaAs photoelectrodes with porphyrins having varying positive charge leads to systematic shifts in the band-edge positions.[30] Other results have shown that absorbed ions can also modify the band-edge positions of a semiconductor photoelectrode.[31] For example, Mallouk and co-workers showed that F doping and surface adsorption on TiO_2 leads to large changes in the band-edge positions.[32] Recent experiments by McFarland and co-workers have shown that incorporation of F into Fe_2O_3 increases the observed photovoltage for water oxidation, also presumably due to the surface dipole and associated band-edge shift.[33]

3.3. Energetics of Semiconductor/Liquid Junctions under Illumination

The free energy that is produced by a semiconductor/liquid contact does not in practice reach the theoretical energy limit dictated by the interfacial energetics discussed above. Instead, the actual free energy obtained depends on the kinetics of the charge carriers in the photostationary state that is produced as a result of illumination of the solid/liquid interface.[27a] In the solid-state physics formalism, the free energy generated by the semiconductor is given by the difference between the hole and electron quasi-Fermi levels under illumination, that is, by the free energy difference between the majority carriers and the photoexcited minority carriers (Figure 5c). The quasi-Fermi level is simply a description of the electrochemical potential of one carrier type at a time (i.e., either electrons or holes) under nonequilibrium (e.g., illuminated) conditions, using Fermi−Dirac statistics to describe separately the populations of electron and of holes.[34] The prefix *quasi-* refers to the fact that thermalization of the excited carriers is a fast process, leaving the collection of holes (and electrons) each in quasi-thermal equilibrium under steady-state illumination. True equilibrium can be reached only in the dark, through slower conduction-band to valence-band recombination processes, at which point a single Fermi level describes the statistical distribution of all carriers. The degree of splitting between the electron and hole quasi-Fermi levels under no net current flow is referred to as the open-circuit voltage (V_{oc}) and can be measured experimentally in suitable systems.[34a−c]

The magnitude of the photovoltage that is generated by a semiconductor/liquid junction determines the photoelectrochemical reactions that can be driven by that system. Even if the appropriate band-edge positions of the semiconductor straddle the water oxidation and reduction levels, water splitting is not possible unless the photovoltage exceeds 1.23
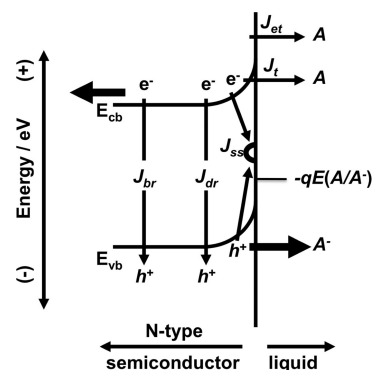
Figure 7. Recombination pathways for photoexcited carriers in a semiconductor photoelectrochemical cell held at open circuit can be broken down into at least five different categories, represented by the thin arrows in the diagram. The electron−hole pairs can recombine through a current density associated with radiative or nonradiative recombination in the bulk of the semiconductor (J_{br}), depletion-region recombination (J_{dr}), surface recombination due to defects (J_{ss}), tunneling current (J_t), and electron-transfer current associated with majority carriers traversing the interfacial barrier (J_{et}). Electron collection by the back contact and hole collection by the redox couple (e.g., oxidation of water to O_2) are processes that contribute positively to device efficiency, and these are depicted by thick black arrows.[26a] Reproduced with permission from ref 26a. Copyright 2005 American Chemical Society.

V.[11,35] This can be explained in a kinetic framework by the principle of microscopic reversibility, in that the rates of the forward, fuel-forming reactions must exceed the sum of the reverse, fuel-consuming, rates.[35a,36] Understanding and controlling the relevant kinetic processes that affect the photovoltage is essential in the design of efficient semiconductor photoelectrodes. These kinetic processes govern the respective electron and hole concentrations at the interface under quasi-equilibrium conditions, and can be broken down into five different categories (Figure 7). The photogenerated charge carriers can (1) recombine in the bulk of the solid (J_{br}), (2) recombine in the depletion region (J_{dr}), (3) tunnel through the electric potential barrier near the surface (J_t), (4) thermally surmount the interfacial potential barrier (thermionic emission) (J_{et}), or (5) recombine at defects (trap states) at the semiconductor/liquid interface (J_{ss}).[18] In some cases, for example for well-surface-passivated silicon single crystals, all of the mechanisms except the fundamentally limiting bulk recombination (J_{br}) can be suppressed.[27a,37] Such devices generate the maximum possible voltage in the photostationary state. In other cases, surface recombination

(J_{ss}) or charge transfer across the interface (J_{et}) dominates the recombination processes.[26d]

The analytical expression for the photovoltage (V_{oc}) generated at a semiconductor/liquid junction is given by the ideal diode equation solved for the situation at zero net current:

$$V_{oc} = (nk_BT/q) \ln(J_{ph}/\gamma J_s) \qquad (5)$$

where n is the diode quality factor, k_B (m^2 kg s^{-2} K^{-1}) is Boltzmann's constant, T (in K) is the temperature, q (C) is the charge on an electron, J_{ph} (A m^{-2}) is the photocurrent density, J_s is the saturation current density, which is related to the sum of the recombination pathways outlined above, and γ is the ratio of the actual junction area to the geometric surface of the electrode (i.e., the roughness factor).[38] As will be discussed in more detail below, this relationship implies a decrease in V_{oc} at room temperature of ≥ 59 mV for each 10-fold increase in γ. Section 8 provides further discussion about the effects of surface roughness on the photoelectrode performance. This equation also shows that the photovoltage is dependent on the illumination intensity, with a higher photon flux leading to more minority carriers and hence to a larger splitting of the quasi-Fermi levels.[39]

When any of the recombination currents 2–5 contribute significantly to J_s, these rate processes limit the photovoltage of the device, and thus limit the ability to drive photoelectrochemical reactions (Figure 7). This point is critically important, in that it is often remarked that if a semiconductor meets the thermodynamic requirements regarding the position of the valence and conduction bands with regard to the redox potentials of HER and OER, this semiconductor should drive the unassisted photoelectrolysis of water. A semiconductor can only drive the photoelectrolysis of water if recombination is sufficiently suppressed such that the quasi-Fermi level splitting and, hence, the photovoltage, exceeds 1.23 V under illumination. Note also that, in optimized semiconductors (e.g., single crystal silicon or GaAs), the maximum attainable photovoltages are typically ~0.4 V smaller than the band gap of the semiconductor.[26a]

A key challenge in the development of water splitting devices is to fabricate semiconductor photoelectrodes for water oxidation and/or reduction that have bulk and surface properties such that the generated photovoltage reaches the fundamental bulk-recombination limit. The kinetics of charge transfer from a bare semiconductor surface to a redox species in solution depends both on the number of electrons (or holes) at the semiconductor surface and on the energetics of the semiconductor band edges.

Consider the well-studied case of an n-type semiconductor in the dark, in contact with an electrolyte that contains a redox couple and is under external potential control.[27c] The electron concentration at the surface of an n-type semiconductor, n_s, is determined through a Boltzmann-type relationship by the difference between the potential applied to the electrode, E, and the flat-band potential, E_{fb}:

$$n_s = N_d e^{q(E_{fb}-E)/k_BT} \qquad (6)$$

where N_d is the concentration of donor atoms. At forward bias, n_s increases exponentially with the application of a negative potential, resulting in a net current across the semiconductor/liquid interface. The net flux of electrons from the conduction band to acceptors dissolved in solution is given by the rate law:

$$J(E) = -qk_{et}[A]n_s \qquad (7)$$

where J is the current density (A cm^{-2}), k_{et} is the electron-transfer rate constant (cm^4 s^{-1}), and [A] is the acceptor concentration (cm^{-3}). Unlike the case for metallic electrodes, the surface electron concentration is explicit in the rate law for electron transfer at semiconductor electrodes. Hence, application of a potential to an ideally behaving semiconductor electrode interface effects a change in the observed current density (i.e., the charge-transfer rate) by changing the electron concentration at the surface of the solid, as opposed to changing the rate constant, or the energetics, of the interfacial charge-transfer process. In the dark, few minority carrier holes are present, so their contribution to the rate can be neglected. This majority-carrier electron-transfer process is a source of detrimental recombination current, and in practical devices it is minimized by introduction of a large electrostatic barrier at the semiconductor surface.[25b]

The kinetics of minority carrier charge transfer under illumination—i.e. useful current—can be analyzed using a similar kinetics framework.[35a] The surface minority-hole concentration for an n-type semiconductor is described by the energy difference between the hole quasi-Fermi level and the valence band edge.[40] Like the case in the dark, the rate of forward hole transfer, from the n-type semiconductor to the solution, is related to the concentration of holes at the semiconductor surface. Furthermore, the driving force for hole transfer to the solution is dictated by the energy difference between the valence band edge and the redox level of the species in solution (for water splitting, this is H_2O or OH^-, depending on the pH) and is independent of the light intensity or potential applied to the electrode, provided that the semiconductor remains in depletion. If the potential of the valence band edge is sufficiently positive of the formal potential of redox couple to give rise to a large electron-transfer rate constant, this condition can be considered a "built-in" overpotential for driving a given redox reaction.[26c]

4. Photocathodes for Hydrogen Evolution

Photocathodes used for a water splitting cell need to supply sufficient cathodic current to reduce protons to H_2 and must be stable in aqueous environments. In addition, to successfully reduce protons to H_2, the potential of the conduction band edge of the photocathode must be more negative than the hydrogen redox potential. The mechanism for the HER is pH dependent: at low pH, the HER proceeds primarily by the reduction of protons, whereas at high pH, water is primarily reduced to produce hydroxide ions.[41] The overall reactions are shown in eq 8.

$$\begin{aligned} 2H^+ + 2e^- &\rightarrow H_2 & \text{(low pH)} \\ 2H_2O + 2e^- &\rightarrow H_2 + 2OH^- & \text{(high pH)} \end{aligned} \qquad (8)$$

As has been summarized earlier, a semiconductor brought into contact with a liquid electrolyte phase will experience Fermi level equilibration with the electrochemical potential (E_{redox}) of the liquid by transferring charge across the interface. For a p-type semiconductor, the bands bend in such a way that photogenerated electrons are driven toward the interface, while holes are swept into the bulk of the solid. Photoexcitation thus injects electrons from the solid into solution. This cathodic current may, to some extent, protect the surface of the semiconductor from oxidation. For this

reason, p-type semiconductors can be expected to be more stable than their n-type counterparts.

Many p-type semiconductors have been investigated as electrochemical photocathodes for the HER, but the scope of this review will be limited to those that have been most thoroughly investigated or that have received attention relatively recently. Work has also been performed on regenerative photoelectrochemical systems and on splitting HBr or HI (which require a smaller overall potential difference to drive the decomposition reaction), which provides useful insights for water splitting applications.[42]

4.1. Photocathode Materials

GaP has an indirect band gap of 2.26 eV, with band edges that straddle the hydrogen reduction potential. The n-type form of this material is unstable in aqueous solution, but p-GaP is stable for extended periods of time under reducing conditions.[43] Memming demonstrated the ability of GaP to produce H_2 positive of the H^+/H_2 thermodynamic potential. One of the drawbacks of GaP is that it has small minority-carrier diffusion lengths relative to the absorption depth of visible light in the solid.[44] Recent work using a regenerative ferrocenium/ferrocene redox system has demonstrated that structuring this material, by etching macropores, increases the photocurrent of n-GaP, and similar strategies should be applicable to p-type materials.[45]

InP has a band gap of 1.35 eV, which makes it a good solar absorber; however the scarcity and high demand of indium limit the commercial viability of the material, at least in traditional wafer format.[46] Using Ru catalyst islands on the surface of oxidized InP, Heller et al. were able to achieve 12% solar to chemical conversion for the production of H_2.[47] By electrodepositing Rh and Re on p-InP electrodes, efficiencies of 13.3% and 11.4% were obtained, respectively (efficiencies were calculated as the ratio of energy that could be produced in an ideal fuel cell using the photoelectrochemically produced H_2 and the solar irradiance striking the photocathode).

Turner and other researchers have systematically studied the properties of $GaInP_2$, whose band gap of 1.83 eV is large enough to split water. Although the potential of the conduction band edge of $GaInP_2$ is more negative than the hydrogen reduction potential, the valence band potential is negative of the oxygen potential, so an additional bias is needed to effect the overall decomposition of water.[48] Some success was achieved in shifting the VB edge more positively by modifying the surface with quinolinol groups.[31a] Measurements in a variety of different electrolyte pHs has indicated that p-$GaInP_2$ is most stable under acidic conditions.[15c]

With a band gap of 1.12 eV, p-Si is a desirable p-type small band gap absorber for possible use in dual band gap p/n-PEC water splitting configurations.[29] Several groups have demonstrated that planar p-Si photocathodes, combined with a variety of metal catalysts, can be used to reduce the voltage required to electrochemically produce H_2.[49] Photon to hydrogen conversion efficiencies as high as 6% (under low-level monochromatic 633 nm illumination) have been reported for p-Si decorated with Pt nanoparticles.[49b] Si is stable in acidic conditions, but surface oxidation can occur over extended periods of time. Passivation of the Si surface by covalent attachment of methyl groups has been shown to improve the stability of p-Si photocathodes.[29,50]

Currently, II−VI semiconductors such as CdTe and $CdIn_{1-x}Ga_xSe_2$ (CIGS) dominate the thin film photovoltaics market. These materials have band gaps that can be controlled by modifying their composition and processing. Several different groups have investigated the properties of II−VI semiconductors, and have used them to split HI and HBr with relatively high efficiencies. Bard and co-workers made single crystals of the group VI selenides and used them to split HI in water, using methyl viologen as a redox shuttle for the hydrogen evolution process.[42,51] Parkinson et al. used molybdenum and tungsten diselenide anodes, along with InP cathodes coated with noble metal catalysts, to split HBr with an efficiency of 7.8% (based on the amount of free energy stored).[14c] Other work showed that during HI decomposition, H_2 bubbles formed at the crystal steps of WSe_2, while I_2 was produced over the flat surfaces of the crystal.[52] The Wrighton group tested p-WS_2 for a variety of PEC reduction reactions, and achieved 6−7% efficiency, and very high open-circuit voltages for hydrogen production, through the use of platinum catalysts.[53] More recently, several groups have reported new ways to create thin film photocathodes by controlling the stoichiometry of copper chalcopyrites. $CuIn_xGa_yS_2$ materials are interesting because they have direct band gaps that can be adjusted by modifying the In:Ga ratio (ranging between 1.52 to 2.5 eV).[54] Work by Fernandez et al. demonstrated that p-type films of $CuIn_{1-x}Ga_xS_2$, fabricated by sputtering the materials onto Mo-coated glass and then sulfurizing the electrodes, have the appropriate energetics to split water at moderate pH (5−7). Miller et al. made $CuGaSe_2$ ($E_g = 1.65$ eV) films that had nonideal band-edge alignment for photoassisted water splitting, but nevertheless exhibited very high photocurrents.[24c] Work by Valderrama showed that the onset for cathodic current was negative of the H_2 reduction potential and that V_{fb} was 0.168 V vs SCE (~0.4 V vs NHE, more positive than H^+/H_2).[55] Cuprous oxide has a direct band gap of 2.0 eV, and can be fabricated by several different methods including thermal oxidation, sputtering, and electrodeposition.[56] Although Cu_2O has been used as both a photoanode and a photocathode, the VB edge of Cu_2O is located at ~0.9 V vs NHE,[15a] making it ineffective for oxygen evolution.[57] Additionally, Cu_2O is unstable with respect to photocorrosion in aqueous conditions, and has a relatively low electrical conductivity. The favorable band gap of Cu_2O thus makes it a more likely candidate for use in a regenerative photoelectochemical cell.[57,58]

4.2. Effects of Catalyst Particles on Photocathode Surfaces

Although several semiconductors have band-edge positions that are appropriate for the photoelectrochemical reduction of water, the kinetics of HER on the bare semiconductor surface generally limit the efficiency of this reaction.[41] Overcoming this kinetic limitation requires a stronger driving force, i.e. an overpotential, to drive the desired chemical reaction. In turn, the overpotential lowers the usable voltage output, and hence lowers the efficiency of the photocathode.[59] Addition of a catalyst to the surface (often in the form of a nanoparticulate metal film) can improve the kinetics of the reaction.[60] Additionally, if the metal is deposited such that the metal particles are discontinuous and smaller than the wavelength of incident photons, the metal film will effectively be optically "transparent" and not significantly affect the light absorption properties of the semiconductor.[61] To date, the most efficient system based on a p-type semiconductor has been achieved using p-InP decorated with

Pt catalyst islands, yielding a 13.3% conversion efficiency to hydrogen.[47]

Semiconductors that are coated with discontinuous films of metal nanoparticles behave essentially like the semiconductor alone in contact with a redox couple, albeit with the catalytic activity of the metal coating. This result is different from the behavior of a continuous metal film on a semiconductor surface, which forms a Schottky barrier whose height is determined by the metal/semiconductor interface and whose energetics are independent of the solution. Two approaches have been advanced to explain this phenomenon. The first, developed by Heller, is based on the fact that alloying the metal with H_2 can change the work function of the metal and hence increase the semiconductor/metal barrier height.[62] Because the catalyst material has equilibrated its Fermi level with the H^+/H_2 redox potential, the driving force for the reduction reaction will only depend on the barrier height of the semiconductor/metal junction.[8c] The need for nonuniform metal films can be explained by the fact that a continuous film would limit the amount of light absorbed by the semiconductor, and would thus reduce the photocurrent from the system.

Another approach to explaining the hybrid behavior of nanoscale metal particles on semiconductors is to treat the semiconductor/liquid interface as a junction with an inhomogeneous barrier height. It is well-known that semiconductor-metal Schottky junctions exhibit "Fermi level pinning," in which the barrier height (ϕ_b) of the junction is much lower than the theoretical difference in work functions between the two materials. However, if the diameters of the metal particles are comparable to the depletion width of the semiconductor, under certain conditions, the high barrier height liquid junction can dominate the band bending in the semiconductor. The predicted size dependence on the effective barrier height has been observed for n-Si/Ni/electrolyte systems.[63] In the regime in which the scale of the metal particle is comparable to, or smaller than, the depletion width of the semiconductor, the current density depends strongly on the band bending of the semiconductor as well as on the spatial dependence of the barrier height.[63] If the metal nanoparticles are small and well dispersed on the semiconductor surface, the effective barrier height of the system will be controlled by the semiconductor/electrolyte interface, so the effect of the metal on the energetics of the system will be "pinched off" (Figure 8).

Both the H_2 metal-alloy and "pinch-off" theories offer reasonable explanations for the behavior of semiconductor/metal electrolyte systems with metal island nanoparticles. Work by Szklarczyk et al. and by Rossi et al. provides experimental evidence that supports the "pinch-off" theory.[21,63] Szklarczyk's work systematically investigated photoelectrocatalysis for a variety of different metals on p-Si, and found that the photoevolution of H_2 for a variety of metal nanoparticle catalysts was directly related to the metal's exchange current density for H_2 evolution in the dark.[21]

Theoretically, the pinch-off effect can be exploited to promote the desired catalytic reaction at the semiconductor surface. A metal has a continuum of energetic states, so a higher density of majority carriers exists in the metal than in the semiconductor. This should enable the facile transport of minority carriers into the metal, where the electrons can more easily be used in the redox reaction. Decoration of the semiconductor surface with pinched-off catalysts will also protect the semiconductor from corrosion, because the surface
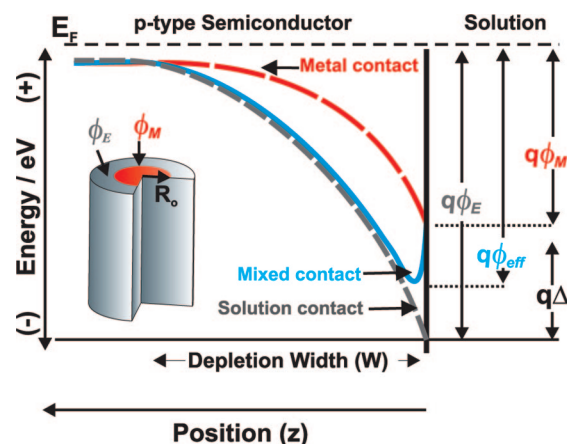
Figure 8. Plot of the valence band edge as a function of position in a p-type semiconductor behind a mixed barrier height contact, where Φ_E is the barrier height between the semiconductor and solution and Φ_M is the barrier height between the semiconductor and the metal. $\Delta \equiv \Phi_E - \Phi_M$ (the difference in barrier height between the two contacting phases), and W is the depletion width behind an unperturbed region of the liquid contact. A particle with a sufficiently small radius will be pinched off, meaning that the effective barrier height (Φ_{eff}) across a mixed contact junction will be much larger than that of the low barrier height metal contact. The extent to which pinch off occurs in a given system depends on Δ, the band bending, and the depletion width in the semiconductor.[63]

concentration of minority carriers will be decreased in the semiconductor if the carriers are preferentially transported through the catalyst islands. It is well documented that the addition of Pt nanoparticles to a p-type semiconductor surface significantly lowers the overpotential required to evolve H_2, but these systems are often limited by low photovoltages.[49b] A more detailed understanding of the interface of semiconductor/metal/aqueous systems may help to improve the efficiencies of photocathode devices by exploiting this "pinch-off" phenomenon.

While several promising candidate materials exist for the photocathode of a solar water splitting device, more work is needed to simultaneously optimize both the photoconversion efficiency of the semiconductor and the rate of catalysis of the HER. This issue will be discussed in greater detail in section 8.

5. Photoanodes for Water Splitting

An oxygen evolving photoanode material must be an n-type semiconductor, such that the electric field generated by band bending drives holes toward the surface. The material must have a band gap and band-edge positions that are suitable for use in a single or multiple band gap system, as well as electrical properties such as doping and resistivity that allow for efficient collection of charge carriers. Additionally, the material needs to be stable under water oxidization conditions, and if the interfacial kinetics of the OER are determined to be rate limiting, an oxygen evolution catalyst must be placed on the electrode surface.

Due to the requirement of stability under oxidizing conditions, most of the photoanode materials that have been investigated are metal oxides or metal oxide anions (oxometalates), in pure, mixed, or doped forms. A general trend in the electronic structures of these oxides and oxometalates is that the valence band (VB) consists of O 2p orbitals, and the conduction band (CB) is formed by the valence orbitals

of one or more metals. An implication of this trend is that, especially in ionic crystals, the potential of the VB edge stays relatively unchanged at 3.0 ± 0.5 V vs NHE for most metal oxides and oxometalates including TiO_2, $SrTiO_3$, WO_3, Fe_2O_3 and ZnO (Figure 2).[64] Metal ions, either as bulk matrix or dopant species, serve to tune the CB position, and hence the band gap.

Upon photoexcitation and charge separation of an n-type semiconductor, minority carriers (holes) in the VB diffuse to the semiconductor−electrolyte interface to oxidize water. The disparity between the oxygen-centered VB at ∼3.0 V and the OER potential at 1.23 V vs NHE presents a major challenge for the development of high-performance photo-anode materials. Thus much of the excess ∼1.77 eV absorbed by the oxide is wasted by thermal relaxation. Unfortunately, few semiconductors satisfy both requirements of electronic structure and stability for photoanodes; thus most examples of functioning photoanodes convert sunlight to O_2 at relatively low efficiencies.

In the following sections, we discuss first several classes of photoanode materials that have been shown to produce oxygen under illumination. Second, we outline several efforts at effecting full water splitting using a single oxide photo-electrode, and describe the corresponding limitations. Third, we describe strategies that have been used to increase the sensitivity of oxides to visible light. Finally, we discuss general factors that have led to improved photoanode performance, implying appropriate strategies for moving forward.

5.1. Transition Metal Oxides as Photoanodes

Several classes of transition metal oxide materials have been shown to satisfy some of the requirements for efficient photoelectrochemical oxygen evolution. The redox-active metal ions in metal oxide photoanodes can include early transition metals, e.g., Ce(IV), Ti(IV), Zr(IV), Nb(V), Ta(V), as well as d^{10} configuration ions, e.g., Zn(II), Ga(III), Ge(IV), Sn(IV) and Sb(V). Additionally, group 1 through 3 metal ions can be added as inert components to help produce specific crystal structures. TiO_2 has been extensively studied following the experiment by Fujishima and Honda,[7] and has also played a central role in dye-sensitized solar cells (DSSCs).[65] However, the potential of the CB edge of TiO_2 lies slightly positive of the HER potential and therefore electrons in the CB do not effect the net reduction of water into H_2,[65,66] unless the photoelectrode is operated under non-standard-state conditions (e.g., with a gradient in pH between the photoanode and cathode).[7,67] This limitation can be overcome by use of the titanates $SrTiO_3$ and $BaTiO_3$, for which the addition of Sr^{2+} and Ba^{2+} cations results in the perovskite structure, and moves the potential of the CB edge more negative than NHE. When loaded with appropriate H_2 evolution cocatalysts such as Rh or Pt, $SrTiO_3$ fully decomposes water, using near-UV photons, with internal quantum yields that approach unity.

As an isoelectronic compound to $SrTiO_3$, $NaTaO_3$ also adopts the perovskite structure. Partly because of its sizable band gap (4.0 eV), and therefore its greater driving force for H_2 evolution, $NaTaO_3$ exhibits a relatively high activity for water splitting, albeit with deep-UV light. In particular, by doping with 2% La, the surface area of the $NaTaO_3$ crystal can be expanded by a factor of 8, with the emergence of terrace-shaped dislocations that spatially separate the active sites for H_2 (cocatalyzed by NiO) and O_2 evolution.[68] As a

result, this system has yielded an O_2 evolution rate of 9.7 mmol/h in pure water, when illuminated with a 400 W Hg light source.[68b]

The stoichiometric addition of more highly charged metal counterions into titanates, niobates and tantalates tends to produce modified perovskite structures that have intervening O^{2-} layers. Representative photoanodes of this type include $La_2Ti_2O_7$, $K_2La_2Ti_3O_{10}$, $Ba_5Nb_4O_{15}$, $Sr_2Ta_2O_7$ and $Ba_5Ta_4O_{15}$. Nonbridging O atoms in these structures can be viewed as terminal oxo M=O groups, and are believed to form the catalytic center for O_2 evolution.[69] Doping $La_2Ti_2O_7$ with Ba increases the surface concentration of hydroxyl groups, and greatly enhances the rate of water photoelectrolysis. Crystals with pyrochlore-type structures, including $Gd_2Ti_2O_7$, $Y_2Ti_2O_7$ and $Cs_2Nb_4O_{11}$, have been reported to show considerable water splitting activity. By comparison, oxides with d^{10}-configuration ions generally yield far inferior performance for water splitting, due to the higher electrone-gativity of these elements. However, Zn-doped Ga_2O_3 can decompose water with a Ni cocatalyst at a rate analogous to that of the most efficient Ti-, Nb-, or Ta-based photocatalysts. One explanation for this behavior is that the introduction of Zn^{2+} produces p-doping, and thus increases the hole mobility in the VB.[70]

5.2. Photoanode-Based Unassisted Water Splitting

Single band gap semiconductor cells that drive the unassisted photoelectrolysis of water are typically composed of wide band gap n-type semiconductors that can generate the necessary photovoltages needed to drive both the OER and the HER. Such electrodes are presently limited to materials that have band gaps greater than ∼3.0 eV, which sets an upper limit on the attainable solar conversion efficiency at ∼2%.

Several metal oxides with n-type semiconducting proper-ties, such as $SrTiO_3$ and $KTaO_3$, can drive the unassisted photoelectrolysis of water under solar illumination; however, solar-to-chemical conversion efficiencies are <1%.[71] Waki et al. demonstrated that GaN ($E_g \sim 3.4$ eV) could split water with UV illumination, but both the lack of stability of the electrode in aqueous solution and the excess current gener-ated from photocorrosion limit the practicality of using this material.[72] β-Ge_3N_4 is a rare example of a non-oxide photocatalyst that stably effects overall water splitting.[73]

5.3. Photoanodes with a Response to Visible Light

Several strategies can be used to decrease the band gap of oxides and oxometalates that have d^0 or d^{10} configurations. Metal ions that have a strong polarizing capability result in M−O bonds that have substantial covalent character, and thus produce an oxygen-to-metal charge transfer absorption in the visible region.[74] Moreover, the potential of the CB edge can be made more positive through the incorporation of transition metals, whereas introduction of N^{3-} and S^{2-} anions shifts the VB edge to more negative potentials.[75]

The high nuclear charge of Mo^{6+} and W^{6+} enables these ions to form covalent M−O−M networks that are respon-sible for the yellow color of the oxides and of the polyoxo-metalate clusters of these metals. The 2.7 eV band gap of WO_3 results in a CB edge potential slightly positive of NHE (Figure 2); nonetheless, WO_3 can oxidize water to O_2 as a

photoanode[76] or with sacrificial oxidants, without the need for an additional OER cocatalyst. Computational studies suggest that, under working conditions, the WO_3 surface is completely covered by oxygen atoms, with water oxidation taking place via hydroperoxide and hydroxyl intermediates.[77]

The soft and polarizable d^{10} and $d^{10}s^2$ outer shells of Cu^+, Ag^+, Cd^{2+}, Hg^{2+}, In^{3+}, Tl^{3+}, Sn^{2+}, Pb^{2+} and Bi^{3+} have a propensity for mixing into the oxygen-centered VB, and the oxides of these metals appear yellow, red or brown. In_2O_3 is well-known to be an efficient photoanode material, although it is only responsive to near-UV light.[78] Litharge (α-PbO) has a band gap of 1.9 eV, and with the ferri-/ferrocyanide redox couple gives rise to photocurrent over a wide range of the visible spectrum (400 nm < λ < 650 nm).[79] However, during water splitting, PbO is converted into metallic PbO_2, and no O_2 is evolved.[80]

Recently, many colored composite oxides composed of soft metal ions (e.g., Bi^{3+}, Pb^{2+}) have been synthesized. Monoclinic $BiVO_4$ has a band gap of 2.4 eV, resulting from a high-lying VB composed of the Bi 6s and O 2p atomic orbitals.[81] $BiVO_4$ catalyzes O_2 evolution driven either by visible photons or by the oxidant $AgNO_3$, as is the case for the isoelectronic material $PbMo_{1-x}Cr_xO_4$ (E_g = 2.3 eV).[82] For oxides in the series $InVO_4$ (E_g = 1.9 eV), $InNbO_4$ (2.5 eV) and $InTaO_4$ (2.6 eV), potentials of the VB edges are located at ~1.8 V vs NHE. The band gaps of these oxides also straddle the HER and OER potentials.[83] Although H_2 is generated from the photolysis of pure water with a NiO cocatalyst, conflicting results regarding O_2 evolution with these oxides have been published by the same authors.[83,84] $BiYWO_6$ (E_g = 2.7 eV) also effects the stoichiometric splitting of water under visible light.[85] $PbBi_2Nb_2O_9$ possesses a sandwiched perovskite structure with alternating $(Bi_2O_2)^{2+}$ and $(PbNb_2O_7)^{2-}$ layers, and displays a visible-light response for either the HER or OER in the presence of appropriate sacrificial reagents.[86]

Group 7−10 transition metal oxides have been more widely utilized as OER cocatalysts than as bulk photoanode materials, because of the scarcity of the metals and/or the tendency to form partially filled d shells. The VB-to-CB transitions of these compounds are localized d−d transitions. In addition, the unpaired d electrons create low-lying excited states that have energy levels between the VB and CB. The orbitals provide an energy ladder for recombination of charge carriers by nonradiative relaxation processes. For hematite (α-Fe_2O_3), with a band gap of 2.2 eV, optical measurements have revealed that, below the main absorption edge, two weak peaks are present, at 1.4 and 2.0 eV, that can be attributed to crystal field transitions.[87] Consequently, the charge recombination rate in hematite is intrinsically high, and the hole diffusion length is only 2−4 nm,[88] severely impairing the performance of this material as a photoanode. Substantial effort has thus been devoted to the fabrication of thin layers[89] and nanoparticles[90] of hematite, to accelerate charge collection. Grätzel et al. have reported that silicon doping of hematite promotes both its electrical conductivity and the development of dendritic nanostructures.[91] These researchers have thus far attained a short-circuit current density of >3 mA cm^{-2} under AM 1.5G sunlight.[92] Recent work from the Grätzel group (Sivula et al.) has also shown good photoactivity for mesoporous films that were sintered on SnO_2 glass electrodes at high temperatures (~800 °C), demonstrating the ability to form efficient hematite photoanodes from colloidal suspensions.[93] Mixed oxide semiconductors in the Ti−Fe−O system have also been synthesized and characterized.[94] TiO_2 codoped with Cr^{3+}/Sb^{5+} as well as with Rh^{3+}/Sb^{5+} exhibited d−d type band gaps of 2.1−2.2 eV, and showed activity for O_2 evolution in the presence of $AgNO_3$.[82,95] The Sb^{5+} codopant maintained charge balance and the oxidation states of Cr^{3+} and Rh^{3+} in the crystal lattice.

Chalcogenide and pnictide semiconductors have been intensively studied with respect to their physical parameters, but not with respect to their interfacial properties in contact with aqueous electrolytes. These anions are softer bases than O^{2-}, and thus give rise to more negative VB potentials than those of metal oxides. GaN and ZnO are isoelectronic and possess essentially identical wurtzite structures, as well as very similar direct band gaps (3.3−3.4 eV). In contrast, in solid solutions of GaN:ZnO, the two relatively soft ions, Zn^{2+} and N^{3-} interact to generate a new absorption band in the 400−500 nm region.[96] Domen et al. reported that these compounds, along with $Rh_{2-x}Cr_xO_3$, are active and stable photocatalysts for the decomposition of water at pH = 4.5.[97] Photoelectrochemical water oxidation has also been demonstrated using GaN:ZnO and IrO_2 at a potential of ~0.95 V vs RHE.[98] (Oxy)nitrides of Ti and Ta offer further reductions in the band gaps, to values of 2.0−2.5 eV, and rely partially on $AgNO_3$ as a sacrificial reagent for O_2 evolution.[99] In situ IR characterization has indicated that the surface of TaON is covered by an overlayer of Ta_2O_5, which serves as the OER active site and protects the buried N^{3-} anions from oxidation.[100] CdS features an attractive, direct band gap of 2.4 eV, and can thermodynamically drive full water splitting. However, in practice, elemental sulfur or polysulfide are usually the oxidation products.[101] By applying a Nafion film that adsorbs a Ru complex as the OER cocatalyst, photoinduced holes have been rapidly harvested at the CdS surface and passed on for O_2 evolution.[102] The potentials of the VB edge of GaP (E_g = 2.3 eV) is almost equal to the standard OER potential, but GaP can nevertheless function as a photoanode for water oxidation in neutral or basic water. To eliminate photocorrosion, GaP needs to be covered by a protective layer, such as Sn-doped In_2O_3 (ITO), before attachment of an OER cocatalyst such as RuO_2.[103]

5.4. Factors Leading to Improved Photoanode Performance

The development of stable photoanode materials that can absorb visible light is a key challenge for effecting the oxidation of water at semiconductor surfaces. An ideal light absorber would behave as a low-pass color filter, whose extinction coefficient approaches infinity above the band gap of the absorber. Such materials are characterized by their pure, rich color, and include materials that are widely used as pigments, including $BiVO_4$, better known as bismuth yellow, and $CdS_{1-x}Se_x$, known as cadmium red.[104] An indirect band gap results in weaker absorption at longer wavelengths and produces a dull, unsaturated color. In a direct band gap semiconductor, the absorption of incident photons is complete within a surface depth of 100−1000 nm, so charges need only to travel a comparatively short distance to reach the solution. As a result, semiconductors with direct band gaps can be made into nanoparticles or thin films as a path to obtain efficient devices. Unfortunately, it is not easy to predict based on crystal or putative electronic structure whether a semiconductor's band gap will be direct or indirect. For example, although GaN, GaP and GaAs all exist in the

zincblende structure, GaP has an indirect band gap, whereas GaAs and GaN exhibit direct band gaps.

Crystal structures and crystal phases cast profound influence on the properties of oxide semiconductors. For VBs that consist of mostly O 2p orbitals, the electronic coupling between adjacent orbitals is modulated by the dihedral angle, with stronger O 2p–2p couplings contributing to more positive VB edge potentials as well as larger hole mobilities. Accordingly, a more delocalized or "thicker" VB, centered on O 2p orbitals, is facilitated by the 180° Ta–O–Ta angle in $KTaO_3$, compared to the 143° angle in $LiTaO_3$.[105] The cubic perovskite- or ReO_3-type structure is therefore arguably optimized for the purpose of acting as a photoanode material. Indeed, almost all of the highest-performance photoanodes based on Ti, Nb or Ta have a perovskite, or layered perovskite, structure. Isoelectronic materials adopt the same crystal structure, such as the aforementioned pairs $SrTiO_3$/ $KTaO_3$, $PbMo_{1-x}Cr_xO_4$/$BiVO_4$, and ZnO/GaN. Isoelectronic substitution or mixing could thus be a helpful approach to fine-tune the electronic structure of a known material.

Introduction of inert, lattice-mismatching atoms, as in $NaTaO_3$:La and Fe_2O_3:Si, creates crystal defects, and frustrates the growth of large single crystallites. Therefore, various nanostructures can be readily prepared to obtain a high surface area and/or small crystal domains, without special dispersion techniques, possibly allowing for more efficient collection of charge carriers in spite of low mobilities. Additionally, doping that maintains the crystal lattice produces free charge carriers, and thus dramatically increases the electrical conductivity, as in the case of Ga_2O_3: Zn. As an even simpler doping strategy, oxygen vacancy sites as n-type dopants can be produced at higher temperatures and lower O_2 partial pressures. A third type of doping can be considered alloying with an element from the same group. More importantly, like the formation of eutectic mixtures, nonlinear results are often obtained. For instance, doping GaP with 0.5–1% N shrinks its 2.26 eV indirect band gap into a ∼2.1 eV direct band gap,[106] and alloying colorless $PbMoO_4$ with yellow $PbCrO_4$ yields orange or red $PbMo_{1-x}Cr_xO_4$.

From a materials perspective, a huge range of candidate oxides and structured wide band gap materials may have many of the characteristics desired for efficient photoanodic water oxidation. A recent review mentions many of the 130 candidate metal oxides that have been studied for electrochemical water splitting.[107] To sort through these candidates, and seek out new materials, combinatorial methods have been developed to quickly screen large numbers of material combinations.[108] Metal oxide material combinations can be deposited onto electrodes, and automated systems have been used to test for photoactivity under illumination. For example, a metal oxide testing kit has been developed by Parkinson et al. at the University of Wyoming under the name SHArK (Solar Hydrogen Activity Research Kit), to seek out new photoelectrolysis candidates.[108a,109] The kits are being utilized as a research and educational platform for use in high schools and undergraduate/graduate institutions. While such combinatorial efforts hold promise for discovery of new photoanode candidate materials, they should not be considered a substitute for targeted study of known systems or their variations.

6. Dual Band Gap Solar Water Splitting Cells

Honda and Fujishima's photoelectrolysis report suggested that the efficiency of the water decomposition process could be increased by coupling a p-type photocathode to the TiO_2 photoanode.[7] This type of water splitting cell provides an increase in light absorption through the use of a smaller band gap semiconductor, and more importantly, generates enough photovoltage to drive the hydrogen evolution reaction (p/n-PEC, Figure 4b).[14c] The use of TiO_2 as a photoanode material has significant limitations with respect to the amount of photocurrent that can be generated under white light illumination. In addition, with two semiconductor–liquid junctions present, two surface electrocatalysts are required, to reduce the overpotential for each electrode. This constraint is especially relevant at the photoanode, at which the overpotential losses often exceed 0.5 V. The maximum system external quantum efficiency is limited to 50%, because absorption of two photons, one photon per semiconductor material, is required to generate one electron that is capable of fuel production. From a systems perspective, in this arrangement, four photons are required to produce one molecule of H_2, and eight photons are required to produce one molecule of O_2.

6.1. p/n-Photoelectrolysis Cells

Yoneyama et al. constructed a photoelectrolysis cell using an n-type TiO_2 photoanode and a p-GaP photocathode p/n-PEC configuration. Open-circuit voltages were, however, less than the 1.23 V needed to successfully demonstrate unassisted photoelectrochemical water splitting.[110] Stability issues with the p-GaP electrode precluded sufficient evaluation of this cell. Nozik reported unassisted solar water splitting using a back-to-back photoelectrode configuration, again using p-type GaP photocathodes and TiO_2 photoanodes.[14a,b] The dual p/n-PEC cell geometry was termed a "photoelectrochemical diode" and represented a p/n-PEC that contained two semiconductor/liquid junctions (Figure 4b). These devices operated at less than 1% efficiency, and encountered stability issues due to the degradation of the p-GaP photocathodes used to drive the hydrogen evolution reaction. Ohashi et al. also evaluated the n-TiO_2/p-GaP dual band gap system, and calculated a solar to hydrogen conversion efficiency (STH) of ∼0.1% under 50 mW cm^{-2} of illumination.[111] This report also evaluated several p/n-PEC configurations of p-CdTe/n-TiO_2 (STH of 0.04%), p-GaP/n-$SrTiO_3$ (STH = 0.7%), and p-CdTe/n-$SrTiO_3$ (STH = 0.2%). It is important to note that, with a band gap of 3.4 eV, $SrTiO_3$ can split water by itself, albeit with lower overall efficiencies than might be obtainable in a p/n-PEC.[112]

Mettee and Calvin reported a dual band gap p/n-PEC "heterotype" cell that used n-Fe_2O_3 with RuO_2 surface catalysts, and p-GaP with Pt islands, to drive the photoelectrolysis of water.[113] Due to their electrode setup and configuration, the cells were illuminated side-by-side and were wired together externally, thereby halving the photocurrent density compared to a "stacked" cell design. A close comparison was made between this dual band gap cell and the two-step light reactions of natural photosynthesis, to oxidize water and reduce NAD to $NADH_2$. The dual n-Fe_2O_3/ p-GaP cell was run in neutral pH (Na_2SO_4) and in seawater, exhibiting solar-to-hydrogen efficiencies of 0.01% and 0.1%, respectively. The authors noted the poor electrical perfor-

mance and quantum efficiency of the n-Fe_2O_3 as significantly limiting the overall efficiency of the photoelectrolysis process.

An efficient p/n-PEC for the unassisted photoelectrolysis of water was a configuration developed by Kainthla et al. that consisted of a photocathode composed of p-type InP coated with Pt islands, and an n-type GaAs electrode coated with a thin protective MnO_2 layer.[20,114] The photoelectrolysis cell operated at 5 mA cm^{-2} with an overall solar-to-chemical conversion efficiency of 8.2%. Testing of the individual photoelectrodes in separate three-electrode cells indicated short-circuit photocurrent densities over 18 mA cm^{-2} for the MnO_2-protected GaAs electrode and almost 30 mA cm^{-2} for the Pt decorated p-InP photocathode. Although the two curves were not overlaid in the report, it is clear that the operating current density of a "stacked" configuration would have been near 10 mA cm^{-2}, but the cells were illuminated side-by-side, halving the current density. Although the efficiency is impressive, the materials used in this deviced incorporated expensive, non-earth abundant materials (In), with surface bound Pt electrocatalysts, suggesting expensive large-scale production.

Akikusa and Khan reported a water splitting cell that used two wide band gap materials, p-SiC ($E_g \sim$ 2.9 eV) and n-TiO_2 ($E_g \sim$ 3.0 eV).[115] Although n-SiC is prone to photocorrosion in electrolyte solutions,[116] p-SiC is cathodically protected under illumination, and exhibits a remarkably negative conduction band-edge potential (-1.3 V vs NHE) for reducing protons to H_2. A photoelectrode composed of p-SiC coated with Pt islands and a TiO_2 photoelectrode illuminated side-by-side split water with an open-circuit voltage of 1.25 V and an operating current density of 0.05 mA cm^{-2}, for an overall solar-to-hydrogen efficiency of 0.06%. The use of two such wide band gap semiconductors allows for the generation of sufficient photovoltages; however, it limits the available operating photocurrent to the maximum output of the higher band gap photoelectrode.

A homotype dual band gap configuration incorporating both p-type/n-type Fe_2O_3 photoelectrodes was reported by Kahn and Ingler, in which the two photoelectrodes were used in tandem for the unassisted photoelectrolysis of water.[117] Unfortunately, the poor photoresponse and carrier transport of p-type Fe_2O_3 severely limited the efficiency of these cells, resulting in a photocurrent density of 0.1 mA cm^{-2} under 100 mW cm^{-2} illumination (solar-to-hydrogen efficiency of 0.11%). Other devices that used a dual band gap configuration included a two electrode p/n-PEC made from an n-type, nanostructured WO_3 photoanode and a p-type $GaInP_2$ photocathode.[118] The structured device could not split water with light intensities <1 W cm^{-2}, due to a Fermi level mismatch of the two semiconductors and low absorption of visible light by the WO_3. At higher light intensities, a photocurrent of 20 μA cm^{-2} was observed.

6.2. Photoanode−Photovoltaic Cells

An alternative approach to providing additional voltage to a single band gap water splitting device involves integration of a p−n photovoltaic (PV) cell in series with the PEC photoanode material (Figure 4c). Morisaki et al. reported a hybrid TiO_2 photoanode coupled with a p−n junction Si photovoltaic device, by depositing the TiO_2 photoelectrode on top of the PV cell, with the latter protected from the solution by a Pt metal electrode. Light that was not absorbed by TiO_2 could be captured by the p−n Si photovoltaic layer,

and thus provided the additional bias needed for water splitting.[19b] In a single band gap PEC + (PV cell) device, a dark anode or cathode with catalytic properties can be used, or surface-bound catalysts can help drive the hydrogen/ oxygen evolution reactions.

An efficient single band gap n-type photoanode PV-coupled device has been reported by Grätzel and Augustynski, who reported a structured WO_3 photoanode in series with a dye-sensitized TiO_2 solar cell (DSSC).[65] Some features of this cell include the use of a DSSC module to provide the necessary bias to drive the hydrogen evolution reaction at a platinum cathode in series with a WO_3 photoanode. Several patents related to the use of an Fe_2O_3 photoelectrode coupled to a DSSC report efficiencies as high as 2.2%. This work is based upon success with Si-doped nanostructured Fe_2O_3 electrodes deposited on Sn-doped In_2O_3, which have shown incident-photon-to-current efficiency (IPCE) values as high as 42% (at 370 nm) and photocurrent densities (J_{sc}) of 2.2 mA cm^{-2} under 1 Sun illumination.[91] Subsequent work by Brillet et al. used an Fe_2O_3 photoanode that was connected in series to two DSSCs, one of which used a squaraine sensitized cell, followed by an N749 (black dye) sensitized DSSC to form a trilevel tandem configuration.[119] The reported operating photocurrent densities (J_{sc}) were 0.94 mA cm^{-2} with an overall STH of 1.36%.

Miller et al. reported a single band gap device that used a PV layer to provide an additional bias with good stability. The system consisted of a WO_3 semiconductor photoanode coupled to a triple-junction amorphous photovoltaic stack.[19a,120] This configuration utilized a photoactive nanostructured thin film of either WO_3, Fe_2O_3, or TiO_2 that had been deposited using low temperature (<300 °C) reactive sputtering.[19b] The lower temperature deposition of the WO_3 films is an important consideration for both the cost effectiveness of developing this system and for the materials chosen to construct the photoelectrodes. These metal oxide films were sputtered onto an a-Si:Ge tandem PV cell that was electrically connected to a hydrogen evolution catalyst electrode, such as Pt or RuO_2, and ohmically connected to the front metal oxide photoanode. This configuration provides another example of complementary absorbing layers in which the bias provided by the tandem PV cell is buried in a solid-state junction, and utilizes photons with energies that are not absorbed by the metal oxide film. These devices showed operating photocurrent densities of <1 mA cm^{-2} when Fe_2O_3 and TiO_2 were used as photoanodes. Devices that used WO_3 exhibited operating current densities of 0.45 mA cm^{-2}, with solar-to-hydrogen efficiencies of 0.7% while operating for 10 h in acidic media under AM 1.5 illumination. A similar WO_3 photoanode PEC−PV based device was later reported using a triple junction amorphous-Si tandem PV cell to increase the bias voltage, resulting in a solar-to-hydrogen efficiency of 0.6% with generated current densities of 3 mA cm^{-2}.[19a] Miller et al. also have reported the use of a triple junction a-Si solar cell that was coated with $NiFe_yO_x$ and CoMo catalysts to yield 7.8% efficiency.[121] This design is an example of a photovoltaic−photoelectrolysis cell with catalyst-coated electrodes that are essentially wired to an a-Si solar cell. Several other configurations similar to this particular implementation are presented in section 6.4.

6.3. Photocathode−Photovoltaic Cells

A very efficient photoelectrolysis cell that utilizes a direct semiconductor/liquid electrolyte junction is the 12.4% solar

water splitting configuration based on a p-GaInP$_2$ photocathode connected in series to a p–n GaAs junction photovoltaic layer, reported by Khaselev and Turner.[48b] This device was modeled after a solid-state tandem cell and used complementary absorbing layers, with the p-GaInP$_2$ photocathode having a band gap of 1.83 eV to absorb the visible part of the spectrum, while the p–n GaAs, with a band gap of 1.42 eV, absorbed the near-infrared part of the spectrum that was not absorbed by the p-GaInP$_2$ layer. The p-GaInP$_2$ layers were grown using metal–organic chemical-vapor deposition (MOCVD) and were coated with a Pt catalyst. This device can be classified as a dual band gap configuration, with the p-GaInP$_2$ semiconductor/liquid junction carrying out hydrogen evolution with photogenerated minority charge carriers, while the GaAs PV cell layer provided the additional bias needed to drive the oxygen evolution reaction. Although p-GaInP$_2$ has an ideal band gap of 1.8 to 1.9 eV, its band edges do not straddle the HER and OER reactions, requiring a 0.3 V bias to drive the hydrogen/oxygen evolution reactions.[14b] The strategy of using a single semiconductor/liquid junction coupled to a complementary absorbing photovoltaic layer utilizes an unsymmetrical charge-carrier injection configuration. Photogenerated minority carriers (electrons) in the p-GaInP$_2$ layer effect water reduction while majority carriers (holes) generated from the GaAs PV cell effect water oxidation at a Pt electrode. The cell produced 120 mA cm^{-2} at short circuit under 1190 mW cm^{-2} white light illumination, and showed limited long-term stability. The limitations of this configuration include a short photocathode lifetime, in addition to pitting of the GaInP$_2$ electrode surface under focused illumination.[15c] This device configuration also has limited large-scale feasibility due to the expensive vapor-phase epitaxy processing that is required to grow the GaAs p–n junction as well as to produce the GaInP$_2$ photocathode.

6.4. Photovoltaic–Photoelectrolysis Cells

As was mentioned in section 2.3, a PV–PEC configuration is essentially a PV cell that is connected directly to an electrolyzer, with the major difference being that the metal catalyst is deposited directly onto shielded, photoactive semiconductor materials.[121] These semiconductor/metal/liquid junctions can, in principle, operate at any pH, because the semiconducting layers are completely protected from the acidic/alkaline solutions used for photoelectrochemical water splitting, thereby avoiding changes in the semiconductor/liquid junction properties and possible photoelectrode stability issues. The cost of a buried junction configuration, however, is likely to be greater than that of a single photoelectrode, due to the necessity of creating junctions within the electrode, to create the needed photovoltage. Several device structures are presented here to illustrate the efficiency and stability properties of buried junction photoelectrolytic cells.

Khaselev, Bansal, and Turner demonstrated a 16% efficient n/p-GaInP$_2$/GaAs(Pt) and 7.8% triple-junction p–i–n a-Si(Pt) photovoltaic/electrolysis cell configurations.[122] The n/p-GaInP$_2$/GaAs(Pt) design is similar to the earlier reported p-GaInP$_2$/p–n GaAs photoelectrolysis cell with the addition of an additional n-GaInP$_2$ to form two PV cells in series. The n/p-GaInP$_2$/GaAs tandem cell exhibited a $V_{oc} = 2.32$ V under 100 mW cm^{-2} of illumination, $J_{sc} = 13.4$ mA cm^{-2}, and $ff = 0.62$. The cell configurations required a Pt electrocatalyst surface for both the HER and OER reactions.

The cells demonstrated highly efficient solar water splitting cells that incorporate an electrolyzer directly onto the surface of the PV cells and were found to be more efficient than separate electrolyzers coupled to PV cells.

Yamane et al. have recently reported a composite semiconductor electrode for water splitting that used an n-Si/p-CuI/ITO/n–i–p a-Si/n-p GaP/ITO/RuO$_2$ configuration. With this cell, they observed a 2.2 V shift from the anodic current that was observed when only a RuO$_2$ electrode was used to oxidize water.[123] This cell was developed around a photovoltaic structure that used p-CuI/n-Si to generate a high open-circuit photovoltage, with a sputtered ITO ohmic top contact. The RuO$_2$ catalyst layer was prepared on ITO using either an electrodeposition step or a chemical deposition technique, with the latter exhibiting smaller current density under water oxidation conditions. The overall chemical conversion efficiency of this cell was 2.3%, while generating a photocurrent density of 1.88 mA cm^{-2}. This device demonstrates an effective method of integrating photovoltaic junctions within a photoelectrode that is coated with highly active electrocatalysts. For the unassisted photoelectrolysis of water, it was necessary to generate over 2.0 V of potential to drive the reactions at both electrodes. A platinum counter electrode was required for hydrogen evolution, and RuO$_2$ was deposited onto ITO to effect oxygen evolution.

Yamada and co-workers demonstrated a 2.5% STH efficient amorphous-Si triple-junction (PV) device that integrated hydrogen and oxygen evolution catalysts coated on the electrode surface.[124] A Co–Mo alloy was used as the HER catalyst, while Fe–Ni–O was used for the oxygen evolving catalyst. The novelty of this device was that the entire photovoltaic electrolysis cell was built on an ITO electrode and was protected from the solution using epoxy, allowing the entire device to be submerged for testing. The device was operationally stable for 18 h. This device can also be categorized as a buried junction, due to the buried triple junction a-Si photovoltaic stack that was protected from solution by the catalyst layer.

A unique configuration developed by Licht et al. placed an AlGaAs/Si photovoltaic stack on top of a RuO$_2$/Pt dual electrode that was submersed in the electrolyte solution.[24a] This design was essentially a photovoltaic cell connected directly to the electrocatalyst surface components (RuO$_2$ and Pt). However, the system avoided problems of light attenuation due to bubble formation on the photoelectrode surface and avoided any possible photoelectrode degradation due to splitting water at the photoelectrode surface. Impressive solar-to-hydrogen efficiencies of 18% were obtained with good operational stability over >12 h. The cost limitations for this cell are significant when considering the large area of the Pt/RuO$_2$ dual electrode, in addition to the MOCVD-grown AlGaAs/Si photovoltaic junctions needed to provide a large photovoltage.

The best known industrial attempt at a photoelectrochemical system for hydrogen production and storage was developed by Texas Instruments in 1981, and used HBr as the medium, evolving H$_2$ at a photocathode and Br$_2$ at a photoanode.[125] Researchers developed pairs of silicon p–n junction particles that were wired in series to generate enough photovoltage to oxidize Br$^-$ to Br$_2$ and to reduce protons to evolve H$_2$. The H$_2$ and Br$_2$ were stored (hydrogen in a metal hydride and Br$_2$ in solution), and used when needed in a fuel cell to generate electricity. The efficiency of the H$_2$-

Table 1. Mutiple Band Gap Solar Water Splitting Cells

materials and configurations	surface catalyst(s)	cell type	η = (STH) %	references
p-GaP/TiO$_2$	n/a	p/n-PEC	<1	Nozik[14a]
p-GaP/Fe$_2$O$_3$	n/a	p/n-PEC	0.01	Mettee[113]
p-InP/GaAs (MnO$_2$)	Pt (photocathode)	p/n-PEC	8.2	Kainthla[114]
(2)DSSCs/Fe$_2$O$_3$	Pt (anode)	photoanode/(2)PVs	1.36	Brillet[119]
(2)a-Si:Ge/WO$_3$	Pt (photocathode)	photoanode/PV	0.7	Miller[19b]
p-GaInP$_2$/p−n GaAs	Pt (photocathode)	photocathode/PV	12.4	Khaselev[48b]
AlGaAs/Si	Pt/RuO$_2$	(2) PVs	18	Licht[24a]
n/p-GaInP/GaAs	Pt/Pt	(2) PVs	16.5	Khaselev[122]
n-Si-pCuI/n−i−p,a-Si/p−n GaP	Pt/RuO$_2$	(3) PVs	2.3	Yamane[103]

and Br$_2$-generating solar panels was 8.6%, with all reactants and products stored and continually reused in a closed system.

A summary of the various multiple band gap water splitting cell configurations reviewed, photoelectrodes used, and their efficiencies (organized by cell type) is presented in Table 1.

7. Effects of Surface-Attached Catalysts on Photoelectrodes for Water Splitting

Typically, electrolysis requires application of greater than 1.23 V between the anode and the cathode because of the kinetic barriers that are commonly encountered in performing multistep, multielectron reactions. For example, hydrogen evolution from acidic water requires combining two protons and two electrons to make a chemical bond. On most bare semiconductor surfaces, the formation, or reductive desorption of intermediate hydride species presents a large energy barrier to hydrogen production.

The catalytic behavior of a given material (in the dark) can be quantified by the current density that can be passed at a given overpotential. The overpotential is simply the voltage applied to the electrode relative to the redox potential of the relevant couple (e.g., H$^+$/H$_2$) in the electrolyte of interest. The overpotential is necessary to drive the kinetically rate-limiting step of the multistep oxidation or reduction reaction. In the case of photoelectrodes, the electrocatalytic behavior is convoluted with the device properties of the semiconductor/liquid contact, and will affect the overall performance of a photoelectrolysis cell (Figure 9).

A common, and often necessary, strategy to improve the performance of photoelectrochemical devices is to add catalytic units to the surface of the semiconductor. Typically these electrocatalysts are deposited as thin layers or as nanoparticles so as to avoid excessive light absorption or reflection, preserve desired interfacial energetics (e.g., via

"pinch off," see section 4.2, Figure 8), and improve the kinetics of the desired reactions.

Aside from improving the photoelectrode kinetics, the addition of catalyst particles fundamentally changes the energetics of the electron transfer process at the semiconductor surface. As discussed in section 3.1, the excited minority carriers in a pristine semiconductor/liquid junction thermalize in the semiconductor to the band edge level (Figure 5). However, when a metallic catalyst particle is on the semiconductor surface, the minority carriers that participate in the redox reaction come from the catalyst particle, whose Fermi energy is in equilibrium with the minority carrier quasi-Fermi level in the semiconductor, as in a traditional metal−semiconductor Schottky contact.[34a,b] Therefore, the addition of catalyst particles to a bare semiconductor surface can actually lead to a loss in driving force, and thus produces a slower electron-transfer rate constant for the reaction. However, this loss in driving force is often offset by drastically increased catalytic turnover rates, thereby increasing the overall device efficiency.

Figure 9 depicts the effects of surface catalysts on a photoelectrode. For a generic "good" catalyst, ∼100 mV is needed to drive a current density of ∼10 mA cm^{-2}, whereas for a "bad" catalyst ∼600 mV is needed to produce the same current density. In principle, the open-circuit voltage (V_{oc}) produced by use of either catalyst should be the same, because the catalyst has no effect on the thermodynamics of the reaction. However, the fill factor and, hence, overall photoelectrode efficiency are drastically reduced by poor catalyst performance.

7.1. Electrocatalysis for Solar Water Splitting

For use in a water splitting device, a good HER or OER catalyst must satisfy two basic requirements. First, the catalyst must be highly active toward its respective reaction, meaning it must be capable of producing, at a minimum overpotential, large quantities of hydrogen or oxygen as quickly as the absorber can supply electrons or holes to the catalyst. Second, an effective catalyst must be robust enough to maintain its efficiency over time scales relevant to commercial use. Catalysts described in the industrial electrolysis literature largely meet these requirements, although continued research in the area demonstrates that improvements would still be beneficial.

A Tafel relationship describes well the catalytic performance of electrodes for the hydrogen or oxygen evolution half-reactions (eq 9),

$$\eta = b\log(I/I_0) \qquad (9)$$

where η is the overpotential, I is the observed current, and I_0 is the exchange current. The Tafel slope, b, is a measure of the potential increase required to increase the resulting
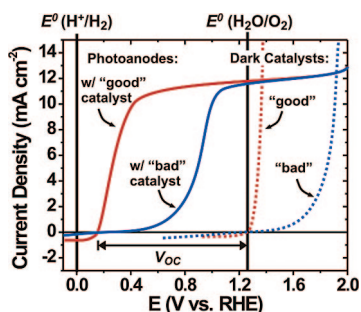
Figure 9. Schematic showing the qualitative effect of surface catalysts on photoanode performance. Dotted curves show the current density vs overpotential relationship for generic "good" and "bad" catalysts. The solid curves show the performance of a hypothetical oxygen-evolving semiconductor photoanode integrated with either a "bad" or "good" catalyst.
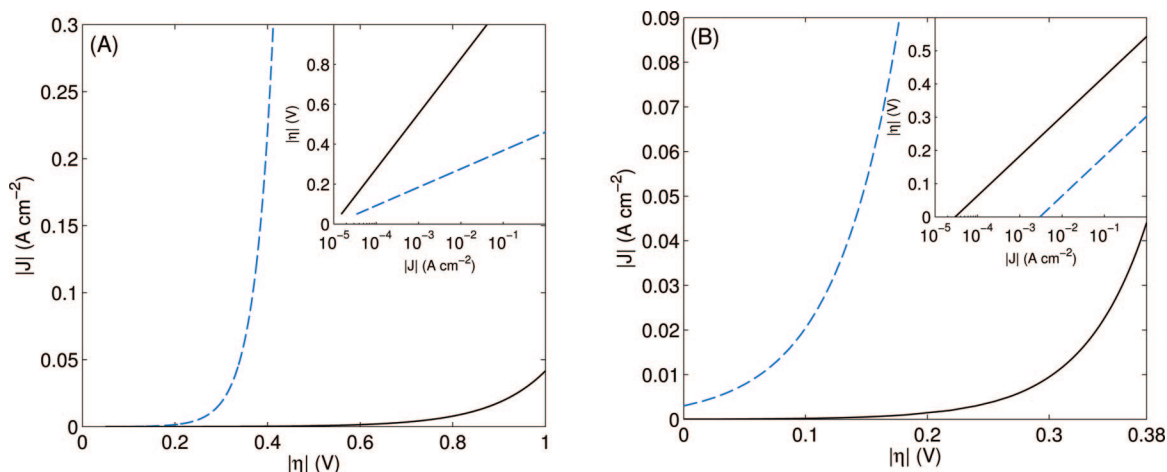
Figure 10. Polarization curves and Tafel plots (inset) illustrating the electronic and geometrical effects of catalysts. (A) Dashed blue: $J_0 = 10^{-5}$ A cm^{-2}, $b = 40$ mV/decade. Solid black: $J_0 = 10^{-5}$ A cm^{-2}, $b = 120$ mV/decade. (B) Dashed blue: $J_0 = 3 \times 10^{-3}$ A cm^{-2}, $b = 120$ mV/decade. Solid black: $J_0 = 3 \times 10^{-5}$ A cm^{-2}, $b = 120$ mV/decade.

current 1 order of magnitude, usually reported in mV/decade. The exchange current corresponds to the intercept at $\eta = 0$, extrapolated from a linear portion of a plot of η versus log(I) (i.e., a Tafel plot). This reaction rate under dynamic equilibrium is also described in terms of geometric area as the exchange current density, J_0 (e.g., A cm^{-2}). Qualitatively, J_0 can be thought of as a measure of how vigorously the forward and reverse reactions occur during dynamic equilibrium, while b is a measure of how efficiently the electrode can respond to an applied potential to produce current. Though researchers often invoke J_0 values alone to describe the catalytic performance of an electrode, the Tafel slope is also an important measure of electrode performance, because it accounts for changes in mechanism at different overpotentials. Taken together, the Tafel slope and the exchange current density can often determine whether improved performance of an electrode after some modification is due to electronic, geometric (surface-area), or combined effects. For example, Figure 10(A) compares two hypothetical catalysts with comparable active surface areas (correlated with J_0) and different electronic activities (correlated with b), whereas Figure 10(B) compares two catalysts with comparable electronic activity but with different active surface areas.

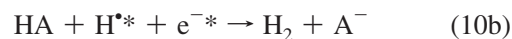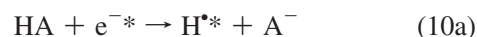## 7.2. Mechanism and Theory of the Hydrogen Evolution Reaction

Many materials that are potentially useful as photocathodes for the HER do not have surfaces that are sufficiently electrocatalytic to support light-driven H$_2$ evolution without a large additional electrical bias. The construction of an efficient device for splitting water with sunlight thus requires the attachment of a more active HER catalyst to the absorber surface. Much of the work on candidate catalysts has come from academic and industrial efforts that have been focused on the development of cheap, efficient water electrolysis systems. An overview of HER catalysis by Trasatti contains an exhaustive description of the available heterogeneous catalysts.[58]

The HER is one of the most well-studied electrochemical reactions. It is understood to proceed by one of two mechanisms,[41] each consisting of two primary steps, as outlined in eqs 10a, 10b, and 10c. The "discharge" step, eq 10a, proceeds in all cases, while only one of 10b or 10c
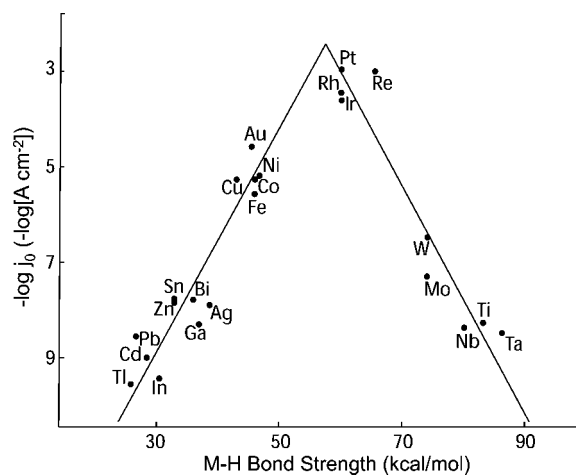
Figure 11. The volcano relation for pure metals in acidic solution (Trasatti).[126] The noble metals Pt and Pd demonstrate exceptionally high activity, with Ni as the most active non-precious metal. Reproduced with permission from ref 126. Copyright 1972 Elsevier.

typically predominates to complete the reaction. The asterisk (*) represents a binding site at the electrode surface, while A$^-$ refers to the conjugate base of the reduced (acidic) proton, namely, H$_2$O in acidic media and OH$^-$ under alkaline conditions.

$$HA + e^- * \rightarrow H^\bullet * + A^- \qquad (10a)$$

$$HA + H^\bullet * + e^- * \rightarrow H_2 + A^- \qquad (10b)$$

$$2H^\bullet * \rightarrow H_2 \qquad (10c)$$

Exchange current densities for the HER on pure metals in acid have been measured by numerous researchers.[126] Plotting these values versus the metal−hydrogen bond strength gives rise to a characteristic pattern, known as the "volcano" relation (Figure 11), where the HER activity increases to a peak value obtained at intermediate bond strengths and then decreases at higher bond strengths.

In highly alkaline media, comparable collected values of the exchange current density are not readily available; rather, the overpotentials required to achieve a set current density were measured for the transition metals by Miles.[127] A plot of such data against periodic group gives a similar volcano
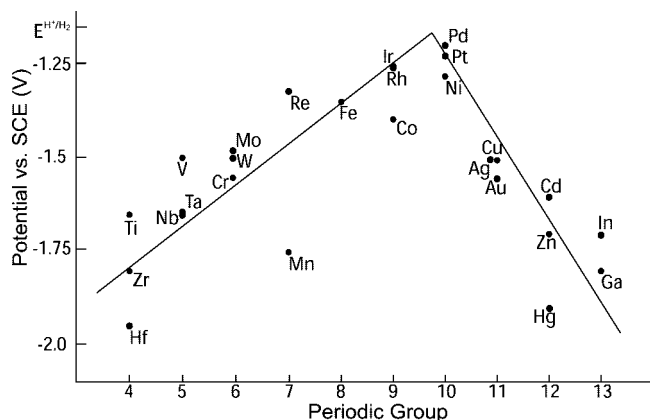
Figure 12. The volcano relation (in 30 wt % base solution) based on potentials required to attain a current density of 2 mA cm^{-2}, as measured by Miles.[127] Reproduced with permission from ref 127. Copyright 1975 Elsevier.

Figure 13. Tafel plots for the following HER catalysts, reproduced from the associated references: bright Ni, Ni−Mo−Cd;[133] bright Ni−Mo;[132c] Ni−Fe, Ni−Co, Ni−Mo;[134] bright WC;[135] RuO$_2$−IrO$_2$;[136] bright Pt.[137] "Bright" refers to electrode surfaces that have been polished such that the electrochemically active area equals the projected area, whereas electrodes not noted as "bright" have not been corrected for electrochemically active surface area. Solid red curves were collected in basic electrolyte, whereas dashed blue curves were collected in acidic electrolyte. Plots of bright Ni and Ni−Mo−Cd were reproduced with permission from ref 133. Copyright 1985 the Royal Society of Chemistry. Bright Ni−Mo, bright WC, and RuO$_2$−IrO$_2$ data was reproduced with permission from refs 132c, 135, and 136, respectively. Copyright 1998, 1987, and 1994 Elsevier. Ni−Fe, Ni−Co, and Ni−Mo data was reproduced with permission from ref 134. Copyright 1993 Springer Science + Business Media. Bright Pt data was reproduced with permission from ref 137. Copyright 1957 American Chemical Society.

relation, with Pt, Pd, and Ni among the most active pure metals (Figure 12). This behavior is consistent with the notion that the predominant HER mechanism for a given metal is the same in acidic and basic media.

Based on the observed volcano relation, the catalytic activity toward the HER is understood to arise from the strength of the interaction between the catalyst surface and adsorbed hydrogen. In the 1950s Gerischer and Parsons independently introduced the first frameworks for understanding the nature of hydrogen catalysis on transition metals on the basis of hydrogen adsorption energies.[128] Both reached the conclusion that the ideal HER electrocatalyst is the one with negligible hydrogen adsorption free energy. The following is a contracted form of Parsons' discussion of why this is the case.
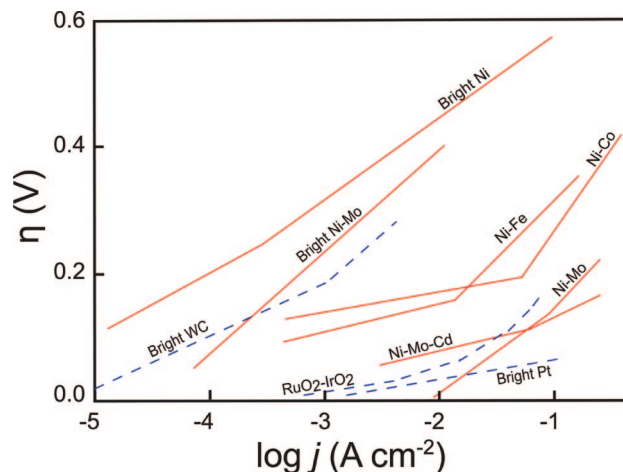
Considering only the discharge step, which all mechanisms share in common, Parsons showed that the exchange current can be described by eq 11:

$$i_0 = \frac{e k_B T}{h} a_{H^+}^{1-\alpha} (\theta^*)^\alpha (1 - \theta^*)^{1-\alpha} e^{-E_a/k_B T} \quad (11)$$

where a_{H^+} is the activity of protons, θ^* is the fractional equilibrium coverage of hydrogen on the metal, E_a is the activation energy for the reaction step, and α is the symmetry factor for the electrochemical energy barrier. The quantity θ^* is determined by the free energy of adsorption. In case of $\alpha = 0.5$, the maximum rate is attained when both θ^* and $(1 - \theta^*)$ are equal to 0.5, corresponding to coverage of half of the available metal sites by reduced hydrogen and an adsorption free energy of zero, that is, equal stability for both adsorbed and absent hydrogen at adsorption sites.

Parsons showed that all three distinct HER steps obey a similar relation, so that, regardless of the predominant mechanism or rate-limiting step, the maximum exchange current for the reaction is attained when the free energy of hydrogen adsorption is zero, or nearly zero. Extensive experimental work has indeed shown that protons converted to hydrogen on platinum surfaces bind with small adsorption energies.[129]

Unfortunately it is very difficult to use any fundamental parameters of a material to predict hydrogen adsorption energies or resulting HER activities. Recently, though, Nørskov and co-workers have used density functional theory to build a predictive model of HER activity on the basis of calculated adsorption energies.[130] This model was able to

reproduce, with some accuracy, the volcano curve for metal catalysts. Furthermore, the calculations predicted high catalytic activity for certain metal composites and reasonably high activity for edge sites on lamellar MoS$_2$. Both predictions have been supported by subsequent experiments.[131]

7.3. Catalyst Materials for Hydrogen Evolution

Aside from pure metal catalysts, electrochemists have studied myriad other materials for efficient, low-cost hydrogen evolution.[132] These can be divided into two broad categories: metal composites/alloys and compounds that incorporate nonmetallic elements. A few examples are highlighted below, but the reader is directed to the available review literature for a more exhaustive analysis.[58] Several selected catalyst Tafel plots are collected and presented in Figure 13.

Nickel metal has demonstrated high performance when subjected to treatments to increase its active surface area.[138] Accordingly, the majority of examples from the literature of mixed-metal catalysts involve additions of another metal, or metals, to nickel. Of particular importance are the binary mixtures of Ni−Mo[134,139] and Ni−Co,[134,138a] as well as the ternary systems Ni−Mo−Cd[133,140] and Ni−Mo−Fe.[141] Electrochemical studies of such compounds have indicated an enhancement of catalytic activity through geometric, electronic, and mixed (so-called synergistic) effects. Nickel has also been mixed with lanthanum to form bulk intermetallic La$_5$Ni, which is understood to behave as a high surface-area nickel catalyst.[142] In many cases, these materials have been shown to exhibit activity comparable to the noble metals they are intended to replace, with low Tafel slopes extending to

quite high current densities. For example, high surface area Ni—Mo electrodes have been reported to require less than 100 mV of overpotential to achieve a current density of 1 A cm^{-2} in alkaline media for thousands of hours.[139c]

Many mixtures of metals with nonmetal components have been employed in search of a high-activity, low-cost catalyst. Trasatti has studied the electrochemistry and HER catalytic properties of a set of metal oxides, mostly based on RuO$_2$, which show high catalytic activity.[136,143] Among the oxides, the ternary mixture Sr$_x$NbO$_{3-\delta}$ is particularly promising due to its low-cost components and high apparent stability.[144] Sulfides have also been pursued, especially nickel sulfide, which appears to exhibit higher activity and stability under alkaline conditions than pure nickel.[145] Tungsten carbide has been shown to be an active catalyst for the HER,[146] likely due to inhibition by carbon of the formation of a deactivating surface oxide.[135,147] Silicotungstates that have been deposited onto conductive substrates have been reported to give extremely high exchange current densities,[148] although control experiments indicate that this activity is likely due to platinum impurities that were stripped from the counter electrode and plated onto the working electrode.[149]

Platinum and other noble metals have been used extensively as catalysts in proof-of-concept photoelectrochemical HER systems, allowing attainment of ∼13% solar conversion efficiency.[47] In spite of the expansive electrolysis literature, however, only a few examples of working photoelectrochemical HER photocathodes have employed catalysts other than noble metals. Perhaps most notable among these is the integrated device developed by Rocheleau et al., who used a sputtered cobalt—molybdenum alloy cathode in strong alkali.[121] Several cases have also emerged in which other materials perform comparably to or better than platinum in systems that utilize sacrificial agents, rather than a coupled anode, for the necessary reductive equivalent. Kakuta et al., for example, reported that coprecipitated ZnS/CdS produced hydrogen with comparable performance to Pt/CdS when illuminated in the presence of a sacrificial reductant.[150] More recently, Zong et. al reported a MoS$_2$ cocatalyst that, along with CdS, produced hydrogen more efficiently than CdS coated with a platinum cocatalyst, under illumination and in the presence of a sacrificial reductant.[151]

## 7.4. Stability of Catalysts for Hydrogen Evolution

Aside from catalytic activity, stability and long-term performance have been primary concerns for the development of HER electrocatalysts.[152] In general, three broad sources contribute to the degradation of electrode performance over time. The first is corrosion, which is a concern for any material, often taking its toll on electrode activity only over long periods. The second is catalyst poisoning by solution impurities. Only very small amounts of deleterious material are required to significantly deactivate an electrode. Finally, electrode performance can be diminished due to changes in the electrode composition or morphology. These effects can occur over long or short time scales, as with hydrogen absorption in Ni, which begins immediately and progresses as the electrode continues to be used.[153] All three of these degradation mechanisms are intimately dependent on the exact conditions under which the electrode is fashioned and operated, including the electrolyte composition and pH, the cell housing, and the specific operating conditions of temperature, potential, and current density. Though general steps can be taken to eliminate rapid catalyst

deterioration, procedures to fully minimize these deleterious effects must be developed individually for each set of material systems and operating conditions.

7.5. Materials and Mechanism for the Oxygen Evolution Reaction

The exchange current densities for water oxidation on the best known catalysts, such as RuO$_2$, are on the order of J_o ∼1 × 10^{-5} to 1 × 10^{-6} A cm^{-2}.[154] This vast difference in activity relative to the 10^{-3} A cm^{-2} exchange current density of Pt or Pd for H$_2$ production in acid is generally attributed to the more complex intermediate structure and kinetics of an oxide phase, as opposed to a metal surface, for the oxidation of water. As a result, electrodes for the oxidation of water generally must operate at relatively high overpotentials. The activities of such catalysts are thus not well described by the exchange current densities of the materials, but are better understood in terms of the corresponding Tafel slopes and $\eta-J$ behavior (Figure 14). The most active known catalysts for water oxidation that are stable enough for laboratory testing are RuO$_2$ under acidic conditions, and NiCo$_2$O$_4$ or doped lanthanum oxides in alkaline media. Tafel slopes range from 30 mV/decade to 120 mV/decade, while 40 mV/decade is the most common. In general, the Tafel slopes of most catalysts drastically increase at higher current densities, due to several factors, including changes in mechanism, uncompensated resistance from bubble formation, and degradation of the catalyst.[154] Note the high overpotentials as compared to those needed to drive the reduction of water to hydrogen. To pass 1 A cm^{-2} with a highly structured NiCo$_2$O$_4$ catalyst, one would need approximately 300 mV, a large overpotential compared to ∼100 mV required for structured Ni—Mo alloy to produce H$_2$ at the same current density.

The apparent activities of all water splitting catalysts are greatly affected by catalyst preparation, as seen by the great
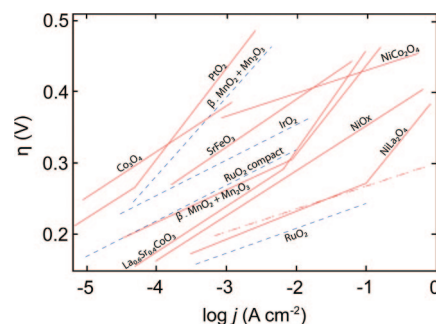
Figure 14. Collected Tafel plots for OER catalysts, adapted from (Trasatti);[165] PtO$_2$;[155] MnO$_x$;[156] Co$_3$O$_4$;[157] NiCo$_2$O$_4$;[158] SrFeO$_3$;[159] IrO$_2$;[160] RuO$_2$ (both "compact" and not);[161] La$_{0.6}$Sr$_{0.4}$CoO$_3$;[162] NiO$_X$;[163] NiLa$_2$O$_4$.[164,165] Solid lines represent alkaline conditions, and dashed lines are under acidic conditions. Current densities are in terms of independently measured electrochemically active surface area. The dot-dashed line, however, shows NiCo$_2$O$_4$ with respect to projected, rather than active surface area, demonstrating that the apparent activity of a catalyst with a high roughness factor increases dramatically if one does not account for the catalytic activity with respect to the active surface area. Data reproduced with permission from ref 165 and from S. Trasatti. Copyright 1981 Elsevier. [Plots of PtO$_2$, MnO$_x$, Co$_3$O$_4$, SrFeO$_3$, IrO$_2$, RuO$_2$ (both forms) and NiLa$_2$O$_4$ were reproduced with permission from refs 155, 156, 157, 159, 160, 161, and 165, respectively. Copyright 1976, 1978 (2), 1979 (2), and 1981 (2) Elsevier. Plots of NiCo$_2$O$_4$, La$_{0.6}$Sr$_{0.4}$CoO$_3$, and NiO$_x$ were reproduced with permission from refs 158, 162, and 163, respectively. Copyright 1979, 1984, and 1978 the Royal Society of Chemistry.]

disparity in activity between two differently prepared RuO_2 catalysts (Figure 14). These differences can be attributed to the method of synthesis and to the conditioning prior to measurement, as well as to the different activities of materials that have widely varying crystallinity. Possible differences in roughness factors and porosities also can contribute to discrepancies in performance of electrodes of the same material. High surface area, Teflon-bonded $NiCo_2O_4$ electrodes, for example, exhibit drastic differences in activity when the projected area is considered relative to when the electrochemically active surface area of the electrode is considered.[158]

A general mechanism for the OER on metal oxides in acidic or alkaline solutions has been proposed on the basis of experimentally measured Tafel slopes.[166] A general mechanism for the OER on metal oxides in acidic solution is given by eqs 12a, 12b, 12c, and 12d.

$$*OH + H_2O \rightarrow [HO*OH] + H^+ + e^- \quad (12a)$$

$$[HO*OH] \rightarrow HO*OH \quad (12b)$$

$$HO*OH \rightarrow O*OH + e^- + H^+ \quad (12c)$$

$$2O*OH \rightarrow 2*OH + O_2 \quad (12d)$$
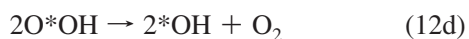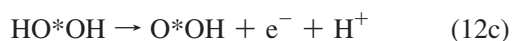
The primary discharge of either water (in acid) or hydroxide (in base) to oxidize a surface-active site (asterisk) is the first step, eq 12a corresponding to a Tafel slope of 120 mV/decade. The result is an unstable intermediate species, designated in square brackets in eqs 12a and 12b. After further chemical conversion to a more stable surface species (eq 12b; 60 mV/decade), the surface is oxidized further (eq 12c; 40 mV/decade). Oxygen is finally liberated from the reaction of two highly oxidized surface sites (eq 12d). This mechanism makes no distinction between the oxygen intermediates that arise from the oxide lattice or from water species. Indeed, the oxide lattice has been shown to participate in the oxidation, with isotopically labeled RuO_2 and $NiCo_2O_4$ surfaces evolving various isotopologues of O_2.[167]

7.6. Theory for the Activity of Oxygen Evolution Catalysts

The activity of oxidation catalysts can be generally understood by the ability of the surface oxide to transition between different valencies to effectively catalyze the oxidation of water. Rasiyah and Tseung proposed that O_2 evolution follows a metal oxide redox transition, and hypothesized that catalysts that undergo such transitions close to the reversible potential for oxygen evolution should possess the highest activity.[168] These two researchers demonstrated a linear correlation between the minimum potential required for oxygen evolution and their lower oxide/higher oxide redox potentials. Trasatti departed from this theory, relating the catalytic activity to the metal−oxygen bond strength on the surface of the oxides.[169] A "volcano" plot, analogous to that observed for the HER, consequently results from correlating the overpotential at a fixed current density to the enthalpy of a lower-to-higher oxide transition (Figure 15). Left of the apex of the volcano plot, the required overpotential increases as the strength of the oxide-intermediate interaction increases. Materials to the right of the apex are easily oxidized, and thus they have a high coverage of the absorbed intermediate, increasing the overpotential for oxygen evolution. Those
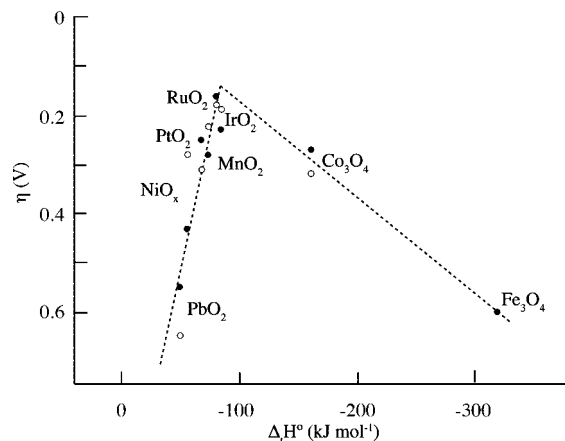
Figure 15. OER volcano plot from Trasatti.[169] Closed circles: in acid. Open circles: in alkaline media. Data reproduced with permission from ref 169. Copyright 1980 Elsevier.

oxides near the apex of the curve (RuO_2, IrO_2) possess optimized bond strengths for the catalysis.

Neither Trasatti nor Tseung relate their observations to any rate-determining step in a mechanism for water oxidation. Tamura and co-workers have correlated experimental activation energies with those calculated from consideration of the ligand-field stabilization energy of complex intermediates formed on the surface during O_2 evolution.[170] More recently, Nørskov et al. implemented density functional theory calculations to model the energetics of the OER on rutile-type oxides.[171] A rudimentary volcano curve was derived, relating the oxygen-evolving activity to the binding energy of various oxygen species on the active oxide surface.

7.7. Catalyst Materials for Oxygen Evolution

A major technological advance in oxygen evolution electrocatalysis came with H. Beer's 1965 patent on the dimensionally stable anode, abbreviated DSA.[172] These electrodes are highly active for electrocatalytic oxidation reactions and also are resistant to chemical and electrochemical degradation. DSAs generally consist of an active component metal oxide, usually RuO_2 and/or IrO_2, thermally decomposed on an inert support, such as Ti. To date, electrodes for water oxidation in acid have not strayed far from this composition: precious metal oxides (RuO_2 and IrO_2) stabilized by inert, inexpensive metal oxides (e.g., TiO_2, SnO_2, Ta_2O_5, ZrO_2) for optimal performance and stability.[173] However, due to the expense of precious metals, nickel operated in hot alkaline solution remains the anode of choice in commercial electrolyzers.

Most interest in conductive metal oxides for oxygen evolution has focused on four classes of crystal structures: dioxides, spinels, perovskites, and pyrochlores.[174] Typical catalysts of the first class include RuO_2 and IrO_2, whereas members of the second class include Co_3O_4 and $NiCo_2O_4$. The third class includes doped lanthanum oxides, such as $NiLa_2O_4$ and $LaCoO_3$, and the fourth class consists of materials such as $Pb_2Ru(Ir)_2O_7$. For more information, the reader is encouraged to consult the extensive review literature.[165,166,174,175]

With respect to OER catalysts in photoelectrolysis systems, it is possible that metal oxide photoanodes can provide enough overpotential to drive the oxidation of water without a catalyst, because the oxide valence band edge potentials are generally very positive of the O_2/H_2O equilibrium

potential. For example, under AM 1 illumination, WO_3 is able to oxidize water at >0.6 V negative of the thermodynamic potential.[76] However, most metal oxide semiconductors, including WO_3, possess wide band gaps, and if a lower band gap oxide that absorbed in the visible and had a less positive valence band potential was used as a photoanode, a catalyst would probably be useful to provide more favorable kinetics for water oxidation.

In practice, the use of oxidation catalysts in existing devices that use light to split water has been largely limited to Pt, either physically deposited on a photoanode surface or used as a "dark" counter electrode, so that the OER can occur separately from the photocathode surface. The choice of Pt as an OER catalyst is not optimal, as a large applied overpotential is required to drive the oxidation of water at $\sim$10 mA cm^{-2} operating current density.[176]

Although the use of oxidation catalysts has been limited in devices fabricated to date, Grätzel and co-workers have observed improvements in the photocurrent−potential response of Fe_2O_3 after it had been treated with $Co(NO_3)_2$, a precursor for Co_3O_4.[91] By deposition of approximately one monolayer of cobalt catalyst on the surface, an 80 mV increase in V_{oc} was observed, accompanied by an increase in maximum observed internal quantum yield from $\sim$37% to $\sim$45%. Pyrolysis of the deposited precursor onto the surface resulted in a decrease in activity, attributed to the aggregation of catalyst particles. Zhong and Gamelin observed a similar increase in the rate of photoelectrochemical O_2 evolution[177] upon electrodeposition in pH 7 phosphate buffer of an amorphous cobalt oxide (CoP_i) catalyst.[178] Additionally, Choi and co-workers observed increased anodic photocurrent from illuminated ZnO electrodes upon photodeposition of a CoP_i catalyst at neutral pH.[179] More information on this cobalt-based water oxidation catalyst is available in the recent literature.[180]

7.8. Stability of Catalysts for Oxygen Evolution

Although it is important to consider catalyst performance, the long-term stability of the conductive metal oxides is also a relevant parameter. The tendency toward anodic dissolution of the metal oxides can be predicted based on thermodynamics.[181] Precious metal dioxides, such as RuO_2 and IrO_2, are more stable in acid, while anodic dissolution occurs in base. Hence, spinels and perovskites are recommended for use in base.[174] Although RuO_2 is widely considered the most active material for water oxidation, this compound is generally unstable at high overpotentials. RuO_2 readily dissolves as ruthenate in basic solutions, or even as volatile RuO_4 if the potentials for the oxidation of surface sites to Ru(VI) or Ru(VIII), respectively, are reached. RuO_4 has been shown to form simultaneously with O_2 evolution on Ru metal at moderate overpotentials ($\sim$200 mV) in acidic media.[182] To minimize anodic corrosion, ruthenium oxide can be stabilized by the addition of an inert metal oxide such as SnO_2 or TiO_2, as in a DSA, or by mixing with IrO_2.[183]

The processing temperature and method of preparation of the material also play major roles in the stability of oxides. Materials that are prepared at higher temperatures, and that have high crystallinity, generally show more stability than amorphous, "hydrous" films that are formed at lower temperatures.[184] However, lower overall catalytic activity, resulting from a lower number of active sites, often accompanies an increase in crystallinity. The optimal trade-off between activity and stability for RuO_2 thus appears to

occur for catalysts synthesized at intermediate temperatures of $\sim$450 °C.[185]

## 7.9. Applications of Electrocatalysts to Solar Water Splitting

There is no shortage of HER and OER catalyst options available at present. However, the particular concerns involved with the attachment of catalysts directly to semiconductor surfaces place significant constraints on which of the known systems can, or should, be utilized. The following section outlines some of the concerns that are unique to semiconductor/catalyst systems.

Several considerations make the development of catalyst materials that are useful in systems for splitting water, and coupling those catalysts to light-absorbers, different from the use of such catalysts in standard electrolysis. One of the most important differences is that light-coupled electrolysis requires absorbers that have large areas, to maximize the capture of the solar flux. If the catalyst is to be deposited directly on the absorber surface, this drastically reduces the requirements for current production per unit geometric area. Consequently, commercial electrolysis systems run at current densities as high as 1 A cm^{-2}, whereas a light-coupled HER apparatus only need run at 10−20 mA cm^{-2}, about a hundred-fold smaller flux.

Concomitant with reduced material performance requirements, however, come more stringent requirements on the cost of catalyst materials, because comparatively more mass of catalyst will likely be required to cover the relevant area. Many of the problems with the stability of conventional metal, metal composite, and metal oxide electrodes can be attributed to the requirement of running electrolyzers at high current densities, at elevated temperatures, and in highly caustic environments. None of these are required of semiconductor-coupled systems. Thus, catalysts in these cases can possibly be expected to be more robust.

For electrolyzers, Tafel slopes are preferred relative to exchange current densities as metrics for evaluating the activity of dark electrolysis catalysts, due to the Tafel slope's ability to distinguish between electronic and geometric (surface-area) effects on apparent catalyst performance. Indeed, this distinction is particularly important for electrolysis systems because, at the overpotentials required to drive their characteristically high current densities, the benefits of extremely high surface areas tend to erode due to the generally high Tafel slopes ($\sim$120 mV/decade) of geometrically enhanced materials. At the comparatively low current densities required by light-coupled water splitting, however, there is less incentive to focus on electronic performance gains relative to geometric gains. Figure 16 shows that, for current densities of tens of mA cm^{-2}, a hypothetical water splitting catalyst that has relatively high surface area (high observed J_0), but has a low fundamental electronic activity (high Tafel slope), outperforms a catalyst that has a lower surface area but a higher electronic activity.

Another way to describe this behavior is to evaluate the photocurrent density required to match the incoming solar flux in a light-coupled cell, based on the geometrical (i.e., projected) area of the cell. A highly structured catalyst or absorber substrate could possess an active surface area that is, conservatively, ten times greater than its projected area. This means that the coupled catalysts would only need to produce a few mA cm^{-2} of electrochemically active catalyst area. As a result, high surface-area forms of cheap, abundant
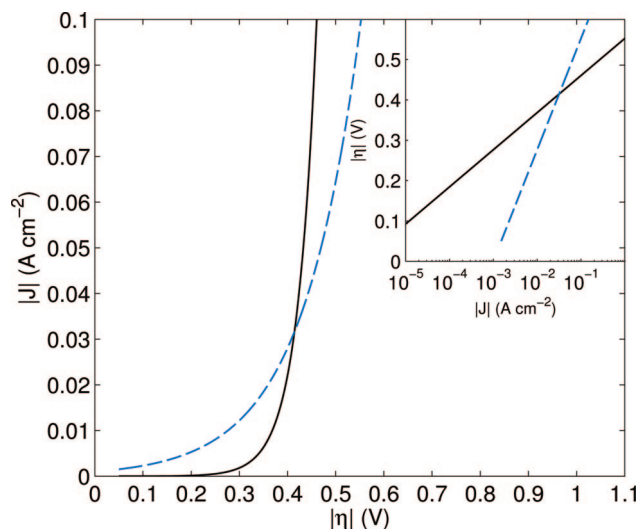
Figure 16. Polarization curve and Tafel plot (inset) of two hypothetical HER catalysts. Dotted blue: $J_0 = 10^{-6}$ A cm^{-2}, $b = 40$ mV/decade. Solid black: $J_0 = 10^{-3}$ A cm^{-2}, $b = 120$ mV/decade. Note the crossover point at ~ 0.4 V and ~ 30 mA cm^{-2}, where the high-b catalyst overtakes the high-J_0 one in HER performance.

materials, e.g. pure nickel, could be sufficient to provide the catalysis necessary for these types of systems.

Photoelectrolysis catalysts, however, must not obscure a significant fraction of light incident on the surface of a device. Transition metal or conductive metal oxide catalysts will often absorb or reflect some of the light, decreasing the resulting efficiency. A thick, continuous catalyst layer with an extremely high surface area like that found in industrial electrolyzers, while perhaps sufficiently catalytic, is useless in practice for a semiconductor-coupled system, because the metal overlayer will absorb or reflect nearly all of the incident light. Concerns over both catalytic activity and light absorption/reflection can perhaps be mitigated together either by the development of catalysts that are transparent (e.g., a transparent conducting oxide) or by moving toward systems in which both the absorber and the catalyst are micro- or nanostructured, so as to produce a high surface area for both. Another option is to actually take advantage of the optical properties of an absorber or a catalyst material so as to enhance rather than diminish light absorption.[186]

Another consideration that is unique to light-coupled water splitting systems is the set of restrictions on the deposition of catalysts that is imposed by the nature of the absorber material. In particular, high-temperature and/or metallurgical preparation methods are not likely to be useful, due to the likelihood of undesired reactions with the absorber medium under such conditions, e.g. silicide formation for metallic catalysts on Si semiconductors at high temperatures. Instead, vacuum (evaporation, sputtering) and solution-phase (electro- and electroless) deposition processes are likely necessary to protect the integrity of the absorber. This constraint renders many of the most active and robust dark HER and OER catalysts inaccessible, unless alternative processing methods can be developed to create materials that have comparable catalytic activity and stability.

A third key consideration that is unique to light-coupled water splitting systems is the necessity of intimately contacting the semiconductor with the catalyst material. In the case of semiconductor/liquid junctions, for example, it will be important to ensure that highly rectifying or appropriately "pinched off" contacts are made between the semiconductor

and the metal. Furthermore, interfacial energy states created at metal−semiconductor contacts could enhance interfacial recombination losses, giving rise to decreased voltages and resulting in losses in efficiency.

8. Micro- and Nanostructural Effects on the Efficiency of Photoelectrodes

Recently much interest has been directed toward the utilization of micro- and nanostructured electrodes for solar energy conversion, in the form of either photovoltaics or direct photoelectrolysis cells.[45,91,187] The primary advantage commonly associated with a structured electrode, compared to a planar system, is the decoupling of the directions of light absorption and charge-carrier collection.[38,188] The distance that a minority carrier can diffuse before recombining is termed the diffusion length (L_D) and is defined as eq 13:

$$L_D = \sqrt{D\tau} \tag{13}$$

where τ is the minority-carrier lifetime and D is the minority carrier diffusion coefficient. The diffusion coefficient is related to the minority-carrier mobility, μ (m^2 V^{-1} s^{-1}), by the Einstein relation, eq 14:

$$D = \frac{\mu k_B T}{q} \tag{14}$$

In a traditional, planar solar cell, the direction of light absorption is the same as that of charge-carrier collection. Thus, to build an efficient cell, the absorber must be thick enough to absorb all the light, but also must be of sufficient electronic quality (i.e., purity and crystallinity) such that the excited minority carriers that are photogenerated deep within the sample are able to diffuse to the surface, where they can be collected. This constraint requires that $L_D \geq 1/\alpha$ (i.e., the absorption length), where α is the absorption coefficient of the semiconductor near the band gap energy. To achieve sufficient diffusion lengths in a planar geometry, high purity semiconductors with few defects that act as recombination sites generally must be used.

The diffusion length requirement can be decoupled from the absorption length if nonplanar geometries, such as a semiconductor rod array, are implemented (Figure 17). As has been shown by device physics modeling, and demonstrated experimentally in several different configurations,[38,188] high surface area semiconductor structures reduce the distance that minority carriers must travel, and hence enable near-unity collection efficiencies despite short minority carrier diffusion lengths.
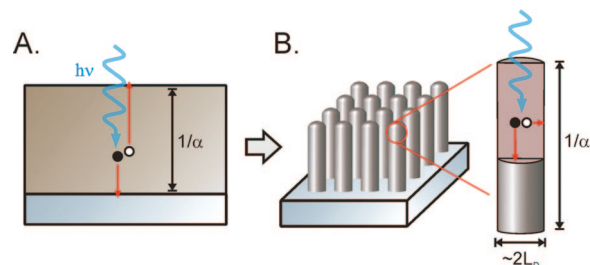
Figure 17. In a planar device (A), photogenerated carriers must traverse the entire thickness of the cell, $\sim 1/\alpha$ (where α is the absorption coefficient), before collection. In a rod-array cell (B), carriers must only reach the rod surface before recombination. L_D is the diffusion length of the photogenerated minority carrier (open circle).

Increasing the junction area of a semiconductor photoelectrode or of a photovoltaic device via nano- or microstructuring has also been shown to reduce the V_{oc} and in this respect is detrimental to device performance.[38,188d] This behavior is expected from a fundamental analysis of the dependence of V_{oc} on the dark and light currents, as presented in section 3 (eq 6). The phenomenon of decreased V_{oc} upon increased junction area results from the reduced splitting in the quasi-Fermi levels when the photogenerated charge carriers are diluted over a large junction area.[34] This situation holds even in the ideal case when surface recombination is negligible and recombination in the bulk (i.e., quasi-neutral) region dominates the system performance. The photovoltage is predicted to decrease by ≥ 60 mV per order of magnitude increase in junction (i.e., solution−semiconductor contact) area.

Practically, this effect means that, to achieve the highest performance from a rod-array electrode, the junction area should be enhanced enough to collect all the carriers (i.e., radius = L_D) but not more. This analysis also suggests that highly nanostructured semiconductor electrodes will suffer from a loss in V_{oc} unless their geometries also significantly enhance light absorption, thereby offsetting the loss from charge-carrier dilution.

Finally, structured semiconductor surfaces should reduce electrocatalysis losses in the form of overpotentials, because of the lower current flux per real area of the electrode. This effect, in principle, might allow for earth-abundant catalysts, with lower activities, and finely spread over a structured electrode, to replace highly active precious metal catalysts.

9. Summary

Numerous combinations of semiconductor materials, electrocatalysts, and cell configurations are available for photoelectrolysis research. As solar fuels research expands, standardizing both research methodologies and characterization techniques becomes paramount for accurate reporting, and ultimately helps to move the field forward into new areas of development and discovery.[16]

In contrast to the use of a single band gap configuration (**S2**) to split water, the use of a dual band gap (**D4**) water splitting cell configuration, where the electric field is generated at a semiconductor liquid junction or through a "buried junction", appears to be the most efficient and robust use of complementary light absorbing materials.[10,11] Multiple junction configurations require innovative contacts and new electrocatalysts. Semiconducting materials continue to be developed, and many of their electrochemical properties remain to be fully understood and optimized.

Recent efforts toward the development of efficient photoelectrolysis devices have centered largely on advances in controlling the size and shape of micro- and nanoscale features of semiconductors and catalysts. The use of structured photoelectrodes lowers material purity constraints by controlling the directionality of charge movement and by controlling the light absorption pathways in the semiconductor. High aspect ratio photoelectrode surfaces also might allow for the use of less expensive catalysts with lowered catalytic activities.

The search for earth-abundant materials that can be used in solar water splitting cells remains an important goal for affordable and environmentally benign methods for energy conversion and storage. Photoelectrode stability continues to be a major challenge for the development of efficient photocathodes and photoanodes. Nature uses a continually renewed dual band gap photosystem to capture light and store the energy in simple sugar molecules. A similar photoelectrosynthetic strategy can be used to decompose water using two semiconductors and store the energy in the simplest chemical bond, H_2.

10. Abbreviations

[A]	concentration of species A
a	activity
AM	Air Mass standardized solar irradiance
b	Tafel slope
CB	conduction band
CIGS	$CdIn_{1-x}Ga_xSe_2$
D	minority carrier diffusion coefficient
D4	PEC classification involving two semiconductors requiring four photons to produce one H_2 equivalent
DSA	dimensionally stable anode
DSSC	dye-sensitized solar cell
E	potential (e.g., volts)
e	signed electron charge
$E°(A/A^-)$	standard potential for the reduction of A to A^-
$E°'(A/A^-)$	formal potential for the reduction of A to A^-
e^-	electron
E_a	activation energy
E_{cb}	conduction band edge energy
E_F	Fermi level
E_{fb}	flat band potential
$E_{F,n}$	quasi-Fermi level for electrons
$E_{F,p}$	quasi-Fermi level for holes
E_g	band gap energy
E_{max}	theoretical maximum potential extractable from a PEC
E_{vac}	vacuum level
E_{vb}	valence band edge energy
ff	fill factor
h	Planck's constant
h^+	hole
$h\nu$	photon
HER	hydrogen evolution reaction
I	current (e.g., amperes)
I_0	exchange current
IPCE	incident photon to current efficiency
I_{sc}	short-circuit current
ITO	tin doped indium oxide
J	current density (e.g., A m^{-2})
J_0	exchange current density
J_{br}	bulk recombination current density
J_{dr}	depletion region recombination current density
J_{et}	current density of interfacial charge transfer
J_g	absorbed photon flux, see eq 1
J_{ml}	current at maximum power output
J_{op}	operating current density
J_{ph}	photocurrent density
J_S	saturation current density
J_{sc}	short-circuit current density
J_{ss}	surface recombination current density
J_t	tunneling current density
k_B	Boltzmann constant
k_{et}	electron-transfer rate constant (e.g., cm^4 s^{-1})
L_D	diffusion length
MOCVD	metal−organic chemical-vapor deposition
n	number of electrons transferred in an electrochemical process
NHE	normal hydrogen electrode
n_s	electron concentration at the surface of a semiconductor
n_{s0}	n_s at zero applied potential

OER	oxygen evolution reaction
p/n-PEC	tandem p/n junction photoelectrochemical cell
PEC	photoelectrochemical cell
PF	power factor
P_{in}	incoming irradiance (power flux)
P_{PA}	power at maximum power point
PV	photovoltaic
q	unsigned electronic charge
$-qE°(A/A^-)$	electrochemical (in eV) of the standard reduction potential of A to A^-
$q\phi_b$	barrier height
RHE	reversible hydrogen electrode
S2	PEC classification involving one semiconductor requiring two photons to produce one H_2 equivalent
SC	semiconductor
STH	solar-to-hydrogen conversion efficiency
T	temperature
UV	ultraviolet
V	voltage
V_{app}	applied voltage
VB	valence band
V_{mp}	voltage at maximum power output
V_{oc}	open-circuit voltage
W	depletion width
α	absorption coefficient
γ	roughness factor
ΔG	free energy change
$\Delta E°$	electrochemical potential difference under standard conditions
η	solar energy conversion effiency; overpotential
θ	fractional surface coverage
λ_g	wavelength corresponding to the band gap energy
μ	minority carrier mobility
μ_{ex}	excess chemical potential generated by a PEC cell, see eq 1
τ	minority carrier lifetime
ϕ	quantum yield

11. Acknowledgments

12. References

(1) *Basic Research Needs for Solar Energy Utilization*; Lewis, N. S., Crabtree, G., Eds.; Office of Science, U. S. Department of Energy: Washington, DC, 2005.
(2) Lewis, N. S. *Science* **2007**, *315*, 798.
(3) Bard, A. J.; Fox, M. A. *Acc. Chem. Res.* **1995**, *28*, 141.
(4) Lewis, N. S. *Nature* **2001**, *414*, 589.
(5) Turner, J. A. *Science* **1999**, *285*, 1493.
(6) Heller, A. *Acc. Chem. Res.* **1981**, *14*, 154.
(7) Fujishima, A.; Honda, K. *Nature* **1972**, *238*, 37.
(8) (a) Bak, T.; Nowotny, J.; Rekas, M.; Sorrell, C. C. *Int. J. Hydrogen Energy* **2002**, *27*, 991. (b) Currao, A. *Chimia* **2007**, *61*, 815. (c) Heller, A. *Science* **1984**, *223*, 1141.
(9) Developments using sacrificial reagents will not be covered in this review, except where promising results with a semiconductor material have only been achieved in this mode.
(10) Bolton, J. R.; Strickler, S. J.; Connolly, J. S. *Nature* **1985**, *316*, 495.
(11) Weber, M. F.; Dignam, M. J. *J. Electrochem. Soc.* **1984**, *131*, 1258.
(12) Werner, J. H.; Kolodinski, S.; Queisser, H. J. *Phys. Rev. Lett.* **1994**, *72*, 3851.
(13) The Schockley−Quiesser limit for maximum solar conversion efficiency is 32% for a 1.4 eV band gap material.
(14) (a) Nozik, A. J. *Appl. Phys. Lett.* **1976**, *29*, 150. (b) Nozik, A. J. *Appl. Phys. Lett.* **1977**, *30*, 567. (c) Fornarini, L.; Nozik, A. J.; Parkinson, B. A. *J. Phys. Chem.* **1984**, *88*, 3238.
(15) (a) Gerischer, H. *J. Electroanal. Chem.* **1977**, *82*, 133. (b) Bard, A. J.; Wrighton, M. S. *J. Electrochem. Soc.* **1977**, *124*, 1706. (c) Khaselev, O.; Turner, J. A. *J. Electrochem. Soc.* **1998**, *145*, 3335.
(16) Chen, Z.; Jaramillo, T. F.; Deutsch, T. G.; Kleiman-Shwarscstein, A.; Forman, A. J.; Gaillard, N.; Garland, R.; Takanabe, K.; Heske, C.; Sunkara, M.; McFarland, E. W.; Domen, K.; Miller, E. L.; Turner, J. A.; Dinh, H. N. *J. Mater. Res.* **2010**, *25*, 3.
(17) (a) Varghese, O. K.; Grimes, C. A. *Sol. Energy Mater. Sol. Cells* **2008**, *92*, 374. (b) Parkinson, B. *Acc. Chem. Res.* **1984**, *17*, 431.
(18) Lewis, N. S. *Acc. Chem. Res.* **1990**, *23*, 176.
(19) (a) Miller, E. L.; Marsen, B.; Paluselli, D.; Rocheleau, R. *Electrochem. Solid-State Lett.* **2005**, *8*, A247. (b) Miller, E. L.; Paluselli, D.; Marsen, B.; Rocheleau, R. E. *Sol. Energy Mater. Sol. Cells* **2005**, *88*, 131.
(20) Kainthla, R. C.; Khan, S. U. M.; Bockris, J. O. M. *Int. J. Hydrogen Energy* **1987**, *12*, 381.
(21) Szklarczyk, M.; Bockris, J. O. M. *J. Phys. Chem.* **1984**, *88*, 1808.
(22) (a) Jahagirdar, A. H.; Dhere, N. G. *Sol. Energy Mater. Sol. Cells* **2007**, *91*, 1488. (b) Shukla, P. K.; Karn, R. K.; Singh, A. K.; Srivastava, O. N. *Int. J. Hydrogen Energy* **2001**, *27*, 135.
(23) Bansal, A.; Tan, M. X.; Tufts, B. J.; Lewis, N. S. *J. Phys. Chem.* **1993**, *97*, 7309.
(24) (a) Licht, S.; Wang, B.; Mukerji, S.; Soga, T.; Umeno, M.; Tributsch, H. *J. Phys. Chem. B* **2000**, *104*, 8920. (b) Park, J. H.; Bard, A. J. *Electrochem. Solid-State Lett.* **2005**, *8*, G371. (c) Marsen, B.; Cole, B.; Miller, E. L. *Sol. Energy Mater. Sol. Cells* **2008**, *92*, 1054.
(25) (a) Pierret, R. F. *Advanced Semiconductor Fundamentals*; Prentice Hall: 2003. (b) Sze, S. M.; Ng, K. K. *Physics of Semiconductor Devices*; John Wiley & Sons, Inc.: Hoboken, NJ, 2007. (c) Tan, M. X.; Laibinis, P. E.; Nguyen, S. T.; Kesselman, J.; Stanton, C. E.; Lewis, N. S. *Prog. Inorg. Chem.* **1994**, *41*, 21.
(26) (a) Lewis, N. S. *Inorg. Chem.* **2005**, *44*, 6900. (b) Memming, R. *Electrochim. Acta* **1980**, *25*, 77. (c) Nozik, A. J.; Memming, R. *J. Phys. Chem.* **1996**, *100*, 13061. (d) Gerischer, H. *J. Electroanal. Chem.* **1983**, *150*, 553.
(27) (a) Lewis, N. S. *J. Electrochem. Soc.* **1984**, *131*, 2496. (b) Fajardo, A. M.; Lewis, N. S. *Science* **1996**, *274*, 969. (c) Fajardo, A. M.; Lewis, N. S. *J. Phys. Chem. B* **1997**, *101*, 11136. (d) Pomykal, K. E.; Lewis, N. S. *J. Phys. Chem. B* **1997**, *101*, 2476.
(28) (a) Hamann, T. W.; Gstrein, F.; Brunschwig, B. S.; Lewis, N. S. *Chem. Phys.* **2006**, *326*, 15. (b) Gerischer, H. *Electrochim. Acta* **1989**, *34*, 1005.
(29) Hamann, T. W.; Lewis, N. S. *J. Phys. Chem. B* **2006**, *110*, 22291.
(30) Hilal, H. S.; Turner, J. A. *Electrochim. Acta* **2006**, *51*, 6487.
(31) (a) Kocha, S. S.; Turner, J. A. *J. Electrochem. Soc.* **1995**, *142*, 2625. (b) Turner, J. A.; Parkinson, B. A. *J. Electroanal. Chem.* **1983**, *150*, 611. (c) Lyon, L. A.; Hupp, J. T. *J. Phys. Chem.* **1995**, *99*, 15718.
(32) (a) Wang, C. M.; Mallouk, T. E. *J. Phys. Chem.* **1990**, *94*, 4276. (b) Wang, C. M.; Mallouk, T. E. *J. Phys. Chem.* **1990**, *94*, 423.
(33) Hu, Y. S.; Kleiman-Shwarscstein, A.; Stucky, G. D.; McFarland, E. W. *Chem. Commun.* **2009**, 2652.
(34) (a) Tan, M. X.; Kenyon, C. N.; Kruger, O.; Lewis, N. S. *J. Phys. Chem. B* **1997**, *101*, 2830. (b) Kruger, O.; Kenyon, C. N.; Tan, M. X.; Lewis, N. S. *J. Phys. Chem. B* **1997**, *101*, 2840. (c) Kenyon, C. N.; Tan, M. X.; Kruger, O.; Lewis, N. S. *J. Phys. Chem. B* **1997**, *101*, 2850. (d) Tan, M. X.; Kenyon, C. N.; Lewis, N. S. *J. Phys. Chem.* **1994**, *98*, 4959.
(35) (a) Kumar, A.; Santangelo, P. G.; Lewis, N. S. *J. Phys. Chem.* **1992**, *96*, 834. (b) Gregg, B. A.; Nozik, A. J. *J. Phys. Chem.* **1993**, *97*, 13441.
(36) Shreve, G. A.; Lewis, N. S. *J. Electrochem. Soc.* **1995**, *142*, 112.
(37) Rosenbluth, M. L.; Lieber, C. M.; Lewis, N. S. *Appl. Phys. Lett.* **1984**, *45*, 423.
(38) Kayes, B. M.; Atwater, H. A.; Lewis, N. S. *J. Appl. Phys.* **2005**, *97*, 11.
(39) Fahrenbruch, A. L.; Bube, R. H. *Fundamentals of Solar Cells*; Academic Press: New York, 1983.
(40) Memming, R. In *Semiconductor Electrochemistry*; Wiley VCH Verlag GmbH: Weinheim, 2001.
(41) Conway, B. E.; Salomon, M. *Electrochim. Acta* **1964**, *9*, 1599.
(42) Levy-Clement, C.; Heller, A.; Bonner, W. A.; Parkinson, B. A. *J. Electrochem. Soc.* **1982**, *129*, 1701.
(43) Memming, R.; Schwandt, G. *Electrochim. Acta* **1968**, *13*, 1299.
(44) Aspnes, D. E.; Studna, A. A. *Phys. Rev. B* **1983**, *27*, 985.
(45) Price, M. J.; Maldonado, S. *J. Phys. Chem. C* **2009**, *113*, 11988.
(46) USGS. *Mineral Commodity Summaries 2010*; U.S. Geological Survey: 2010.
(47) Aharon-Shalom, E.; Heller, A. *J. Electrochem. Soc.* **1982**, *129*, 2865.

(48) (a) Kocha, S. S.; Turner, J. A.; Nozik, A. J. *J. Electroanal. Chem.* **1994**, *367*, 27. (b) Khaselev, O.; Turner, J. A. *Science* **1998**, *280*, 425.

(49) (a) Nakato, Y.; Yano, H.; Nishiura, S.; Ueda, T.; Tsubomura, H. *J. Electroanal. Chem.* **1987**, *228*, 97. (b) Dominey, R. N.; Lewis, N. S.; Bruce, J. A.; Bookbinder, D. C.; Wrighton, M. S. *J. Am. Chem. Soc.* **1982**, *104*, 467.

(50) Bookbinder, D. C.; Bruce, J. A.; Dominey, R. N.; Lewis, N. S.; Wrighton, M. S. *Proc. Natl. Acad. Sci. U.S.A.* **1980**, *77*, 6280.

(51) Fan, F.-R. F.; White, H. S.; Wheeler, B. L.; Bard, A. J. *J. Am. Chem. Soc.* **1980**, *102*, 5142.

(52) Bicelli, L. P.; Razzini, G. *Surf. Tech.* **1983**, *20*, 393.

(53) Baglio, J. A.; Calabrese, G. S.; Harrison, D. J.; Kamieniecki, E.; Ricco, A. J.; Wrighton, M. S.; Zoski, G. D. *J. Am. Chem. Soc.* **1983**, *105*, 2246.

(54) Fernandez, A. M.; Dheree, N.; Turner, J. A.; Martinez, A. M.; Arriaga, L. G.; Cano, U. *Sol. Energy Mater. Sol. Cells* **2005**, *85*, 251.

(55) Valderrama, R. C.; Sebastian, P. J.; Enriquez, J. P.; Gamboa, S. A. *Sol. Energy Mater. Sol. Cells* **2005**, *88*, 145.

(56) Siripala, W.; Ivanovskaya, A.; Jaramillo, T. F.; Baeck, S. H.; McFarland, E. W. *Sol. Energy Mater. Sol. Cells* **2003**, *77*, 229.

(57) de Jongh, P. E.; Vanmaekelbergh, D.; Kelly, J. J. *J. Electrochem. Soc.* **2000**, *147*, 486.

(58) Trasatti, S. *Adv. Electrochem. Sci. Eng.* **1992**, *2*, 1.

(59) Bookbinder, D. C.; Lewis, N. S.; Bradley, M. G.; Bocarsly, A. B.; Wrighton, M. S. *J. Am. Chem. Soc.* **1979**, *101*, 7721.

(60) Bocarsly, A. B.; Bookbinder, D. C.; Dominey, R. N.; Lewis, N. S.; Wrighton, M. S. *J. Am. Chem. Soc.* **1980**, *102*, 3683.

(61) Heller, A.; Aspnes, D. E.; Porter, J. D.; Sheng, T. T.; Vadimsky, R. G. *J. Phys. Chem.* **1985**, *89*, 4444.

(62) Heller, A.; Aharonshalom, E.; Bonner, W. A.; Miller, B. *J. Am. Chem. Soc.* **1982**, *104*, 6942.

(63) Rossi, R. C.; Lewis, N. S. *J. Phys. Chem. B* **2001**, *105*, 12303.

(64) (a) Scaife, D. E. *Sol. energy* **1980**, *25*, 41. (b) Matsumoto, Y. *J. Solid State Chem.* **1996**, *126*, 227.

(65) Grätzel, M. *Nature* **2001**, *414*, 338.

(66) Khan, S. U. M.; Al-Shahry, M.; Ingler, W. B. *Science* **2002**, *297*, 2243.

(67) Nozik, A. J. *Nature* **1975**, *257*, 383.

(68) (a) Kato, H.; Kudo, A. *Catal. Today* **2003**, *78*, 561. (b) Kato, H.; Asakura, K.; Kudo, A. *J. Am. Chem. Soc.* **2003**, *125*, 3082.

(69) Kim, J.; Hwang, D. W.; Kim, H. G.; Bae, S. W.; Lee, J. S.; Li, W.; Oh, S. H. *Top. Catal.* **2005**, *35*, 295.

(70) Sakata, Y.; Matsuda, Y.; Yanagida, T.; Hirata, K.; Imamura, H.; Teramura, K. *Catal. Lett.* **2008**, *125*, 22.

(71) (a) Morisaki, H.; Watanabe, T.; Iwase, M.; Yazawa, K. *Appl. Phys. Lett.* **1976**, *29*, 338. (b) Wagner, F. T.; Somorjai, G. A. *J. Am. Chem. Soc.* **2002**, *102*, 5494. (c) Paulauskas, I. E.; Katz, J. E.; Jellison, G. E.; Lewis, N. S.; Boatner, L. A.; Brown, G. M. *J. Electrochem. Soc.* **2009**, *156*, B580. (d) Mavroides, J. G.; Tchernev, D. I.; Kafalas, J. A.; Kolesar, D. F. *Mater. Res. Bull.* **1975**, *10*, 1023.

(72) Waki, I.; Cohen, D.; Lal, R.; Mishra, U.; DenBaars, S. P.; Nakamura, S. *Appl. Phys. Lett.* **2007**, *91*, 093519/1.

(73) Sato, J.; Saito, N.; Yamada, Y.; Maeda, K.; Takata, T.; Kondo, J. N.; Hara, M.; Kobayashi, H.; Domen, K.; Inoue, Y. *J. Am. Chem. Soc.* **2005**, *127*, 4150.

(74) Woodward, P. M.; Mizoguch, H.; Kim, Y.-I.; Stoltzfus, M. W. In *Metal Oxides: Chemistry and Applications*; Fierro, J. L. G., Ed.; Taylor & Francis: Boca Raton, 2006.

(75) Kudo, A.; Miseki, Y. *Chem. Soc. Rev.* **2009**, *38*, 253.

(76) Hodes, G.; Cahen, D.; Manassen, J. *Nature* **1976**, *260*, 312.

(77) Valdes, A.; Kroes, G. J. *J. Chem. Phys.* **2009**, *130*, 114701.

(78) (a) Liou, F. T.; Yang, C. Y.; Hakim, K.; Levine, S. N. *J. Appl. Electrochem.* **1983**, *13*, 377. (b) Schumacher, L. C.; Mamicheafara, S.; Leibovitch, M.; Dignam, M. J. *J. Electrochem. Soc.* **1988**, *135*, 3044.

(79) Veluchamy, P.; Minoura, H. *Appl. Phys. Lett.* **1994**, *65*, 2431.

(80) Hardee, K. L.; Bard, A. J. *J. Electrochem. Soc.* **1977**, *124*, 215.

(81) Kudo, A.; Omori, K.; Kato, H. *J. Am. Chem. Soc.* **1999**, *121*, 11459.

(82) Shimodaira, Y.; Kato, H.; Kobayashi, H.; Kudo, A. *Bull. Chem. Soc. Jpn.* **2007**, *80*, 885.

(83) Ye, J.; Zou, Z.; Arakawa, H.; Oshikiri, M.; Shimoda, M.; Matsushita, A.; Shishido, T. *J. Photochem. Photobiol., A* **2002**, 79.

(84) Zou, Z. G.; Ye, J. H.; Sayama, K.; Arakawa, H. *Nature* **2001**, *414*, 625.

(85) Liu, H.; Yuan, J.; Shangguan, W. F.; Teraoka, Y. *J. Phys. Chem. C* **2008**, *112*, 8521.

(86) Kim, H. G.; Hwang, D. W.; Lee, J. S. *J. Am. Chem. Soc.* **2004**, *126*, 8912.

(87) (a) Bailey, P. C. *J. Appl. Phys.* **1960**, *31*, S39. (b) Marusak, L. A.; Messier, R.; White, W. B. *J. Phys. Chem. Solids* **1980**, *41*, 981.

(88) Kennedy, J. H.; Frese, K. W. *J. Electrochem. Soc.* **1978**, *125*, 709.

(89) Sartoretti, C. J.; Ulmann, M.; Alexander, B. D.; Augustynski, J.; Weidenkaff, A. *Chem. Phys. Lett.* **2003**, *376*, 194.

(90) Sivula, K.; Formal, F. L.; Grätzel, M. *Chem. Mater.* **2009**, *21*, 2862.

(91) Kay, A.; Cesar, I.; Grätzel, M. *J. Am. Chem. Soc.* **2006**, *128*, 15714.

(92) Tilley, S. D.; Cornuz, M.; Sivula, K.; Grätzel, M. *Angew. Chem., Int. Ed.* **2010**, *49*, 6405.

(93) Sivula, K.; Zboril, R.; Le Formal, F.; Robert, R.; Weidenkaff, A.; Tucek, J.; Frydrych, J.; Grätzel, M. *J. Am. Chem. Soc.* **2010**, *132*, 7436.

(94) (a) Mor, G. K.; Prakasam, H. E.; Varghese, O. K.; Shankar, K.; Grimes, C. A. *Nano Lett.* **2007**, *7*, 2356. (b) Thimsen, E.; Biswas, S.; Lo, C. S.; Biswas, P. *J. Phys. Chem. C* **2009**, *113*, 2014.

(95) Kato, H.; Kudo, A. *J. Phys. Chem. B* **2002**, *106*, 5029.

(96) Maeda, K.; Takata, T.; Hara, M.; Saito, N.; Inoue, Y.; Kobayashi, H.; Domen, K. *J. Am. Chem. Soc.* **2005**, *127*, 8286.

(97) Maeda, K.; Teramura, K.; Lu, D. L.; Takata, T.; Saito, N.; Inoue, Y.; Domen, K. *Nature* **2006**, *440*, 295.

(98) Hashiguchi, H.; Maeda, K.; Abe, R.; Ishikawa, A.; Kubota, J.; Domen, K. *Bull. Chem. Soc. Jpn.* **2009**, *82*, 401.

(99) (a) Hitoki, G.; Takata, T.; Kondo, J. N.; Hara, M.; Kobayashi, H.; Domen, K. *Chem. Commun.* **2002**, 1698. (b) Liu, M. Y.; You, W. S.; Lei, Z. B.; Zhou, G. H.; Yang, J. J.; Wu, G. P.; Ma, G. J.; Luan, G. Y.; Takata, T.; Hara, M.; Domen, K.; Can, L. *Chem. Commun.* **2004**, 2192.

(100) Nakamura, R.; Tanaka, T.; Nakato, Y. *J. Phys. Chem. B* **2005**, *109*, 8920.

(101) Ellis, A. B.; Kaiser, S. W.; Wrighton, M. S. *J. Am. Chem. Soc.* **1976**, *98*, 6855.

(102) Kaneko, M.; Yao, G. J.; Kira, A. *J. Chem. Soc., Chem. Commun.* **1989**, 1338.

(103) Yamane, S.; Kato, N.; Kojima, S.; Imanishi, A.; Ogawa, S.; Yoshida, N.; Nonomura, S.; Nakato, Y. *J. Phys. Chem. C* **2009**, *113*, 14575.

(104) Buxbaum, G. *Industrial inorganic pigments*, 2nd ed.; Wiley-VCH: Weinheim, New York, 1998.

(105) Kato, H.; Kudo, A. *J. Phys. Chem. B* **2001**, *105*, 4285.

(106) Shan, W.; Walukiewicz, W.; Yu, K. M.; Wu, J.; Ager, J. W., III; Haller, E. E.; Xin, H. P.; Tu, C. W. *Appl. Phys. Lett.* **2000**, *76*, 3251.

(107) Osterloh, F. E. *Chem. Mater.* **2008**, *20*, 35.

(108) (a) Woodhouse, M.; Parkinson, B. A. *Chem. Mater.* **2008**, *20*, 2495. (b) Katz, J. E.; Gingrich, T. R.; Santori, E. A.; Lewis, N. S. *Energy Environ. Sci.* **2009**, *2*, 103. (c) Lee, J.; Ye, H.; Pan, S.; Bard, A. J. *Anal. Chem.* **2008**, *80*, 7445. (d) Arai, T.; Konishi, Y.; Iwasaki, Y.; Sugihara, H.; Sayama, K. *J. Comb. Chem.* **2007**, *9*, 574. (e) Jaramillo, T. F.; Baeck, S.-H.; Kleiman-Shwarsctein, A.; Choi, K.-S.; Stucky, G. D.; McFarland, E. W. *J. Comb. Chem.* **2005**, *7*, 264.

(109) Woodhouse, M.; Parkinson, B. A. *Chem. Soc. Rev.* **2009**, *38*, 197.

(110) Yoneyama, H.; Sakamoto, H.; Tamura, H. *Electrochim. Acta* **1975**, *20*, 341.

(111) (a) Ohashi, K.; McCann, J.; Bockris, J. O. M. *Nature* **1977**, *266*, 610. (b) Ohashi, K.; McCann, J.; Bockris, J. O. M. *Int. J. Hydrogen Energy* **1977**, *1*, 259.

(112) Wrighton, M. S.; Ellis, A. B.; Wolczanski, P. T.; Morse, D. L.; Abrahamson, H. B.; Ginley, D. S. *J. Am. Chem. Soc.* **1976**, *98*, 2774.

(113) Mettee, H.; Otvos, J. W.; Calvin, M. *Sol. Energy Mater.* **1981**, *4*, 443.

(114) Kainthla, R. C.; Zelenay, B.; Bockris, J. O. *J. Electrochem. Soc.* **1987**, *134*, 841.

(115) Akikusa, J.; Khan, S. U. M. *Int. J. Hydrogen Energy* **2002**, *27*, 863.

(116) Inoue, T.; Yamase, T. *Chem. Lett.* **1985**, 869.

(117) Ingler, W. B.; Khan, S. U. M. *Electrochem. Solid-State Lett.* **2006**, *9*, G144.

(118) Wang, H. L.; Deutsch, T.; Turner, J. A. *J. Electrochem. Soc.* **2008**, *155*, F91.

(119) Brillet, J.; Cornuz, M.; Le Formal, F.; Yum, J. H.; Gratzel, M.; Sivula, K. *J. Mater. Res.* **2010**, *25*, 17.

(120) Miller, E. L.; Marsen, B.; Cole, B.; Lum, M. *Electrochem. Solid-State Lett.* **2006**, *9*, G248.

(121) Rocheleau, R. E.; Miller, E. L.; Misra, A. *Energy Fuels* **1998**, *12*, 3.

(122) Khaselev, O.; Bansal, A.; Turner, J. A. *Int. J. Hydrogen Energy* **2001**, *26*, 127.

(123) Yamane, S.; Kato, N.; Kojima, S.; Imanishi, A.; Ogawa, S.; Yoshida, N.; Nonomura, S.; Nakato, Y. *J. Phys. Chem. C* **2009**, *113*, 14575.

(124) Yamada, Y.; Matsuki, N.; Ohmori, T.; Mametsuka, H.; Kondo, M.; Matsuda, A.; Suzuki, E. *Int. J. Hydrogen Energy* **2003**, *28*, 1167.

(125) Johnson, E. L. *Tech. Dig.−Int. Electron Devices Meet.* **1981**, 1.

(126) Trasatti, S. *J. Electroanal. Chem.* **1972**, *39*, 163.

(127) Miles, M. H. *J. Electroanal. Chem.* **1975**, *60*, 89.

(128) (a) Gerischer, H. *Bull. Soc. Chim. Belg.* **1958**, *67*, 506. (b) Parsons, R. *Trans. Faraday Soc.* **1958**, *54*, 1053.

(129) Conway, B. E.; Tilak, B. V. *Electrochim. Acta* **2002**, *47*, 3571.

(130) (a) Hinnemann, B.; Moses, P. G.; Bonde, J.; Jorgensen, K. P.; Nielsen, J. H.; Horch, S.; Chorkendorff, I.; Norskov, J. K. *J. Am. Chem. Soc.*

2005, *127*, 5308. (b) Greeley, J.; Norskov, J. K.; Kibler, L. A.; El-Aziz, A. M.; Kolb, D. M. *ChemPhysChem* **2006**, *7*, 1032.

(131) (a) Greeley, J.; Jaramillo, T. F.; Bonde, J.; Chorkendorff, I.; Norskov, J. K. *Nat. Mater.* **2006**, *5*, 909. (b) Jaramillo, T. F.; Jorgensen, K. P.; Bonde, J.; Nielsen, J. H.; Horch, S.; Chorkendorff, I. *Science* **2007**, *317*, 100.

(132) (a) Hu, W. K.; Cao, X. J.; Wang, F. P.; Zhang, Y. S. *Int. J. Hydrogen Energy* **1997**, *22*, 621. (b) Kawashima, A.; Akiyama, E.; Habazaki, H.; Hashimoto, K. *Mater. Sci. Eng., A* **1997**, *226*, 905. (c) de Chialvo, M. R. G.; Chialvo, A. C. *J. Electroanal. Chem.* **1998**, *448*, 87. (d) Hu, C. C.; Weng, C. Y. *J. Appl. Electrochem.* **2000**, *30*, 499. (e) Hu, W. K. *Int. J. Hydrogen Energy* **2000**, *25*, 111. (f) Kaninski, M. P. M.; Stojic, D. L.; Saponjic, D. P.; Potkonjak, N. I.; Miljanic, S. S. *J. Power Sources* **2006**, *157*, 758. (g) Krstajic, N. V.; Jovic, V. D.; Gajic-Krstajic, L.; Jovic, B. M.; Antozzi, A. L.; Martelli, G. N. *Int. J. Hydrogen Energy* **2008**, *33*, 3676.

(133) Conway, B. E.; Bai, L. *J. Chem. Soc., Faraday Trans.* **1985**, *81*, 1841.

(134) Raj, I. A. *J. Mater. Sci.* **1993**, *28*, 4375.

(135) Tsirlina, G. A.; Petrii, O. A. *Electrochim. Acta* **1987**, *32*, 649.

(136) Kodintsev, I. M.; Trasatti, S. *Electrochim. Acta* **1994**, *39*, 1803.

(137) Bockris, J. O. M.; Ammar, I. A.; Huq, A. K. M. S. *J. Phys. Chem.* **1957**, *61*, 879.

(138) (a) Wendt, H.; Plzak, V. *Electrochim. Acta* **1983**, *28*, 27. (b) Endoh, E.; Otouma, H.; Morimoto, T.; Oda, Y. *Int. J. Hydrogen Energy* **1987**, *12*, 473.

(139) (a) Raj, I. A.; Vasu, K. I. *J. Appl. Electrochem.* **1990**, *20*, 32. (b) Brown, D. E.; Mahmood, M. N.; Man, M. C. M.; Turner, A. K. *Electrochim. Acta* **1984**, *29*, 1551. (c) Brown, D. E.; Mahmood, M. N.; Turner, A. K.; Hall, S. M.; Fogarty, P. O. *Int. J. Hydrogen Energy* **1982**, *7*, 405.

(140) (a) Conway, B. E.; Angersteinkozlowska, H.; Sattar, M. A.; Tilak, B. V. *J. Electrochem. Soc.* **1983**, *130*, 1825. (b) Stachurski, D.; Pouli, G.; Pokrzyk, G.; Ripas, J. *Low overvoltage hydrogen cathodes*. U.S. Patent 4,354,915, 1981.

(141) (a) Hu, W. K.; Zhang, Y. S.; Song, D. Y.; Zhou, Z. X.; Wang, Y. *Mater. Chem. Phys.* **1995**, *41*, 141. (b) Jayalakshmi, M.; Kim, W. Y.; Jung, K. D.; Joo, O. S. *Int. J. Electrochem. Sci.* **2008**, *3*, 908. (c) Raj, I. A. *Bull. Electrochem. Soc.* **1999**, *15*, 519.

(142) (a) Hall, D. E.; Sarver, J. M.; Gothard, D. O. *Int. J. Hydrogen Energy* **1988**, *13*, 547. (b) Boonstra, A. H.; Bernards, T. M. N. *J. Less Common Met.* **1990**, *161*, 355. (c) Wu, S. H.; Huang, W. P.; Yang, X. L.; Xie, Q. X.; Wei, W.; Deng, Z. P. *J. Rare Earths* **1999**, *17*, 66.

(143) (a) Krstajic, N.; Trasatti, S. *J. Appl. Electrochem.* **1998**, *28*, 1291. (b) Tavares, A. C.; Trasatti, S. *Electrochim. Acta* **2000**, *45*, 4195. (c) Kircheva, N.; Guerrini, E.; Trasatti, S. *Russ. J. Electrochem.* **2004**, *40*, 1156. (d) Bianchi, I.; Guerrini, E.; Trasatti, S. *Chem. Phys.* **2005**, *319*, 192. (e) Popa, L.; Guerrini, E.; Trasatti, S. *J. Appl. Electrochem.* **2005**, *35*, 1213. (f) Fachinotti, E.; Guerrini, E.; Tavares, A. C.; Trasatti, S. *J. Electroanal. Chem.* **2007**, *600*, 103.

(144) Manoharan, R.; Goodenough, J. B. *J. Electrochem. Soc.* **1990**, *137*, 910.

(145) Nidola, A.; Schira, R. *Int. J. Hydrogen Energy* **1986**, *11*, 449.

(146) (a) Nikolov, I.; Petrov, K.; Vitanov, T.; Guschev, A. *Int. J. Hydrogen Energy* **1983**, *8*, 437. (b) Struck, B. D.; Neumeister, H.; Naoumidis, A. *Int. J. Hydrogen Energy* **1986**, *11*, 541. (c) Wiecek, B. *Pol. J. Chem.* **1996**, *70*, 343. (d) Ma, C. A.; Gan, Y. P.; Chu, Y. Q.; Huang, H.; Chen, D. H.; Zhou, B. X. *Trans. Nonferrous Met. Soc. China* **2004**, *14*, 11.

(147) Tsirlina, G. A.; Petrii, O. A. *Electrochim. Acta* **1987**, *32*, 637.

(148) (a) Keita, B.; Nadjo, L. *J. Electroanal. Chem.* **1987**, *227*, 265. (b) Keita, B.; Nadjo, L.; Haeussler, J. P. *J. Electroanal. Chem.* **1987**, *230*, 85. (c) Keita, B.; Nadjo, L.; Krier, G.; Muller, J. F. *J. Electroanal. Chem.* **1987**, *223*, 287. (d) Keita, B.; Nadjo, L. *J. Electroanal. Chem.* **1990**, *287*, 149.

(149) McKone, J.; Lewis, N. S. California Institute of Technology: Pasadena, CA. Unpublished work, 2009.

(150) Kakuta, N.; Park, K. H.; Finlayson, M. F.; Ueno, A.; Bard, A. J.; Campion, A.; Fox, M. A.; Webber, S. E.; White, J. M. *J. Phys. Chem.* **1985**, *89*, 732.

(151) Zong, X.; Yan, H.; Wu, G.; Ma, G.; Wen, F.; Wang, L.; Li, C. *J. Am. Chem. Soc.* **2008**, *130*, 7176.

(152) (a) Leroy, R. L.; Janjua, M. B. I.; Renaud, R.; Leuenberger, U. *J. Electrochem. Soc.* **1979**, *126*, 1674. (b) Divisek, J.; Mergel, J.; Schmitz, H. *Int. J. Hydrogen Energy* **1982**, *7*, 695. (c) Nidola, A.; Schira, R. *J. Electrochem. Soc.* **1986**, *133*, 1653. (d) Nidola, A.; Schira, R. *J. Electrochem. Soc.* **1986**, *133*, C123.

(153) (a) Huot, J. Y. *J. Electrochem. Soc.* **1989**, *136*, 1933. (b) Rommal, H. E. G.; Moran, P. J. *J. Electrochem. Soc.* **1985**, *132*, 325.

(154) Trasatti, S.; Lodi, G. In *Electrodes of Conductive Metallic Oxides*; Trasatti, S., Ed.; Elsevier: Amsterdam, 1981; Vol. B.

(155) Iwakura, C.; Fukuda, K.; Tamura, H. *Electrochim. Acta* **1976**, *21*, 501.

(156) Morita, M.; Iwakura, C.; Tamura, H. *Electrochim. Acta* **1979**, *24*, 357.

(157) Iwakura, C.; Honji, A.; Tamura, H. *Electrochim. Acta* **1981**, *26*, 1319.

(158) Jasem, S. M.; Tseung, A. C. C. *J. Electrochem. Soc.* **1979**, *126*, 1353.

(159) Matsumoto, Y.; Kurimoto, J.; Sato, E. *J. Electroanal. Chem.* **1979**, *102*, 77.

(160) Gottesfeld, S.; Srinivasan, S. *J. Electroanal. Chem.* **1978**, *86*, 89.

(161) Lodi, G.; Sivieri, E.; Debattisti, A.; Trasatti, S. *J. Appl. Electrochem.* **1978**, *8*, 135.

(162) Bockris, J. O.; Otagawa, T. *J. Electrochem. Soc.* **1984**, *131*, 290.

(163) Miles, M. H.; Huang, Y. H.; Srinivasan, S. *J. Electrochem. Soc.* **1978**, *125*, 1931.

(164) Fiori, G.; Mari, C. M. *Int. J. Hydrogen Energy* **1982**, *7*, 489.

(165) Trasatti, S. *Electrodes of Conductive Metallic Oxides*; Elsevier: Amsterdam, 1980 and1981.

(166) Trasatti, S. In *Electrochemistry of Novel Materials*; Lipkowski, J., Ross, P. N., Eds.; VCH Publishers: New York, 1994.

(167) (a) Hibbert, D. B. *J. Chem. Soc., Chem. Commun.* **1980**, 202. (b) Wohlfahrt-Mehrens, M.; Heitbaum, J. *J. Electroanal. Chem.* **1987**, *237*, 251. (c) Willsau, J.; Wolter, O.; Heitbaum, J. *J. Electroanal. Chem.* **1985**, *195*, 299. (d) Hibbert, D. B.; Churchill, C. R. *J. Chem. Soc., Faraday Trans.* **1984**, *80*, 1965.

(168) Rasiyah, P.; Tseung, A. C. C. *J. Electrochem. Soc.* **1984**, *131*, 803.

(169) Trasatti, S. *J. Electroanal. Chem.* **1980**, *111*, 125.

(170) (a) Arikado, T.; Iwakura, C.; Tamura, H. *Electrochim. Acta* **1978**, *23*, 9. (b) Iwakura, C.; Tamura, H.; Inai, M. *J. Electrochem. Soc. Jap.* **1980**, *48*, 229. (c) Iwakura, C.; Tamura, H.; Inai, M. *J. Electrochem. Soc. Jap.* **1980**, *48*, 173.

(171) Rossmeisl, J.; Qu, Z. W.; Zhu, H.; Kroes, G. J.; Norskov, J. K. *J. Electroanal. Chem.* **2007**, *607*, 83.

(172) (a) Beer, H. B. (Patent) England, 1965; Vol. 1 147−442. (b) Beer, H. B. *J. Electrochem. Soc.* **1980**, *127*, 303C.

(173) Trasatti, S. *Electrochim. Acta* **2000**, *45*, 2377.

(174) Trasatti, S. In *Interfacial Electrochemistry: Theory, Experiment, and Applications*; Wieckowski, A., Ed.; Marcel Dekker: New York, 1999.

(175) (a) Trasatti, S. In *Electrochemical Hydrogen Technologies*; Wendt, H., Ed.; Elsevier: Amsterdam, 1990. (b) Matsumoto, Y.; Sato, E. *Mater. Chem. Phys.* **1986**, *14*, 397.

(176) Bockris, J. O.; Huq, A. *Proc. R. Soc. London A* **1956**, *237*, 277.

(177) Zhong, D. K.; Gamelin, D. R. *J. Am. Chem. Soc.* **2010**, *132*, 4202.

(178) (a) Lutterman, D. A.; Surendranath, Y.; Nocera, D. G. *J. Am. Chem. Soc.* **2009**, *131*, 3838. (b) Kanan, M. W.; Nocera, D. G. *Science* **2008**, *321*, 1072.

(179) Steinmiller, E. M. P.; Choi, K. S. *Proc. Natl. Acad. Sci. U.S.A.* **2009**, *106*, 20633.

(180) (a) McAlpin, J. G.; Surendranath, Y.; Dincă, M.; Stich, T. A.; Stoian, S. A.; Casey, W. H.; Nocera, D. G.; Britt, R. D. *J. Am. Chem. Soc.* **2010**, *132*, 6882. (b) Surendranath, Y.; Dincă, M.; Nocera, D. G. *J. Am. Chem. Soc.* **2009**, *131*, 2615. (c) Kanan, M. W.; Surendranath, Y.; Nocera, D. G. *Chem. Soc. Rev.* **2009**, *38*, 109. (d) Cook, T. R.; Dogutan, D. K.; Reece, S. Y.; Surendranath, Y.; Teets, T. S.; Nocera, D. G. *Chem. Rev.* **2010**, *110*, doi: 10.1021/cr100246c.

(181) (a) Pourbaix, M. *Atlas of Electrochemical Equilibria in Aqueous Solutions*; Pergamon Press: New York, 1966. (b) Tseung, A. C. C.; Jasem, S. *Electrochim. Acta* **1977**, *22*, 31. (c) Barral, G.; Diard, J. P.; Montella, C. *Electrochim. Acta* **1986**, *31*, 277.

(182) Kotz, R.; Stucki, S.; Scherson, D.; Kolb, D. M. *J. Electroanal. Chem.* **1984**, *172*, 211.

(183) Kotz, R.; Stucki, S. *Electrochim. Acta* **1986**, *31*, 1311.

(184) Trasatti, S. *Electrochim. Acta* **1984**, *29*, 1503.

(185) Iwakura, C.; Tamura, H. *Int. J. Hydrogen Energy* **1982**, *7*, 857.

(186) (a) Kelzenberg, M. D.; Boettcher, S. W.; Petykiewics, J. A.; Turner-Evans, D. B.; Putnam, M. C.; Warren, E. L.; Spurgeon, J. M.; Briggs, R. M.; Lewis, N. S.; Atwater, H. A. *Nat. Mater.* **2010**, *9*, 239. (b) Heller, A. *Pure Appl. Chem.* **1986**, *58*, 1189.

(187) (a) Shankar, K.; Basham, J. I.; Allam, N. K.; Varghese, O. K.; Mor, G. K.; Feng, X. J.; Paulose, M.; Seabold, J. A.; Choi, K. S.; Grimes, C. A. *J. Phys. Chem. C* **2009**, *113*, 6327. (b) Goodey, A. P.; Eichfeld, S. M.; Lew, K. K.; Redwing, J. M.; Mallouk, T. E. *J. Am. Chem. Soc.* **2007**, *129*, 12344. (c) Park, J. H.; Kim, S.; Bard, A. J. *Nano Lett.* **2006**, *6*, 24. (d) Beermann, N.; Vayssieres, L.; Lindquist, S. E.; Hagfeldt, A. *J. Electrochem. Soc.* **2000**, *147*, 2456. (e) Yang, X.; Wolcottt, A.; Wang, G.; Sobo, A.; Fitzmorris, R. C.; Qian, F.; Zhang, J. Z.; Li, Y. *Nano Lett.* **2009**, *9*, 2331.

(188) (a) Spurgeon, J. M.; Atwater, H. A.; Lewis, N. S. *J. Phys. Chem. C* **2008**, *112*, 6186. (b) Erne, B. H.; Vanmaekelbergh, D.; Kelly, J. J. *Adv. Mater.* **1995**, *7*, 739. (c) Erne, B. H.; Vanmaekelbergh, D.; Kelly, J. J. *J. Electrochem. Soc.* **1996**, *143*, 305. (d) Maiolo, J. R.; Atwater, H. A.; Lewis, N. S. *J. Phys. Chem. C* **2008**, *112*, 6194. (e) Maiolo, J. R.; Kayes, B. M.; Filler, M. A.; Putnam, M. C.; Kelzenberg, M. D.; Atwater, H. A.; Lewis, N. S. *J. Am. Chem. Soc.* **2007**, *129*, 12346.